AGU PUBLICATIONS

Geochemistry, Geophysics, Geosystems

RESEARCH ARTICLE
10.1002/2014GC005300

Metasomatized ancient lithospheric mantle beneath the young Zealandia microcontinent and its role in HIMU-like intraplate magmatism

J. M. Scott[1], T. E. Waight[2], Q. H. A. van der Meer[2], J. M. Palin[1], A. F. Cooper[1], and C. Münker[3]

[1]Department of Geology, University of Otago, Dunedin, New Zealand, [2]Department of Geosciences and Natural Resource Management (Geology Section), Copenhagen University, Copenhagen K, Denmark, [3]Department of Geology and Mineralogy, University of Köln, Köln, Germany

Key Points:
- SCLM beneath young Zealandia continent is ancient and regionally heterogeneous
- Carbonatite metasomatism has imparted a HIMU-like composition
- Inspected SCLM has not directly contributed to the intraplate basalts

Supporting Information:
- Readme
- Supplementary 1 sample summary
- Supplementary 2 isotope summary
- Supplementary 3 methodology
- Supplementary 4 representative data
- Supplementary 5 isotope modeling

Correspondence to:
J. M. Scott,
james.scott@otago.ac.nz

Citation:
Scott, J. M., T. E. Waight, Q. H. A. van der Meer, J. M. Palin, A. F. Cooper, and C. Münker. (2014), Metasomatized ancient lithospheric mantle beneath the young Zealandia microcontinent and its role in HIMU-like intraplate magmatism, *Geochem. Geophys. Geosyst.*, *15*, 3477–3501, doi:10.1002/2014GC005300.

Received 18 FEB 2014
Accepted 30 JUL 2014
Accepted article online 2 AUG 2014
Published online 2 SEP 2014

Abstract There has been long debate on the asthenospheric versus lithospheric source for numerous intraplate basalts with ocean island basalt (OIB) and high time-integrated U/Pb (HIMU)-like source signatures that have erupted through the Zealandia continental crust. Analysis of 157 spinel facies peridotitic mantle xenoliths from 25 localities across Zealandia permits the first comprehensive regional description of the subcontinental lithospheric mantle (SCLM) and insights into whether it could be a source to the intraplate basalts. Contrary to previous assumptions, the Oligocene-Miocene Zealandia SCLM is highly heterogeneous. It is composed of a refractory craton-like domain (West Otago) adjacent to several moderately fertile domains (East Otago, North Otago, Auckland Islands). Each domain has an early history decoupled from the overlying Carboniferous and younger continental crust, and each domain has undergone varying degrees of depletion followed by enrichment. Clinopyroxene grains reveal trace element characteristics (low Ti/Eu, high Th/U) consistent with enrichment through reaction with carbonatite. This metasomatic overprint has a composition that closely matches HIMU in Sr, Pb ± Nd isotopes. However, clinopyroxene Hf isotopes are in part highly radiogenic and decoupled from the other isotope systems, and also mostly more radiogenic than the intraplate basalts. If the studied spinel facies xenoliths are representative of the thin Zealandia SCLM, the melting of garnet facies lithosphere could only be the intraplate basalt source if it had a less radiogenic Hf-Nd isotope composition than the investigated spinel facies, or was mixed with asthenosphere-derived melts containing less radiogenic Hf.

1. Introduction

An integral part of continental lithosphere is the peridotitic keel that is attached to the base of the crust and isolated from the asthenosphere. The chemical and isotopic composition of this rigid keel, known as the subcontinental lithospheric mantle (SCLM), has consequences for the composition of magmas generated within it or passing through it. Intraplate alkaline volcanic rocks provide one means of assessing the composition of the SCLM because they are commonly derived from the lithospheric mantle and/or entrain a cargo of xenolithic lithospheric material. Mineralogical, geochemical, and isotopic investigation of such xenoliths provides some of the best constraints on the nature, heterogeneity, and thermal structure of the upper mantle [e.g., *McDonough*, 1990; *Pearson et al*., 2003; *Simon et al*., 2008; *Carlson et al*., 2005; *Griffin et al*., 2009b; *Lee et al*., 2011; *Pearson and Wittig*, 2014].

New Zealand is the exposed portion of a largely submerged microcontinent known as Zealandia (Figures 1a and 1b). Zealandia has been repeatedly pierced over the last ~95 Ma by intraplate basaltic magmas with geochemical compositions indicating derivation from a garnet-bearing peridotitic and/or pyroxenite-eclogitic source [*Coombs et al*., 1986; *Barreiro and Cooper*, 1987; *Gamble et al*., 1986; *Baker et al*., 1994; *Price et al*., 2003; *Cook et al*., 2005; *Finn et al*., 2005; *Hoernle et al*., 2006; *Panter et al*., 2006; *Sprung et al*., 2007; *Coombs et al*., 2008; *Timm et al*., 2009; *McCoy-West et al*., 2010; *Timm et al*., 2010; *McGee et al*., 2013; *Scott et al*., 2013]. These basalts have piqued geological interest because many have radiogenic $^{206}Pb/^{204}Pb$ (> 20.5) and unradiogenic $^{87}Sr/^{86}Sr$ (< 0.703) comparable to oceanic island basalts (OIB) such as those from St Helena or the Austral-Cook islands, which are derived from a high time-integrated $^{238}U/^{204}Pb$ (HIMU) mantle reservoir. The HIMU reservoir is one of several distinctive isotopic end-members recognized in

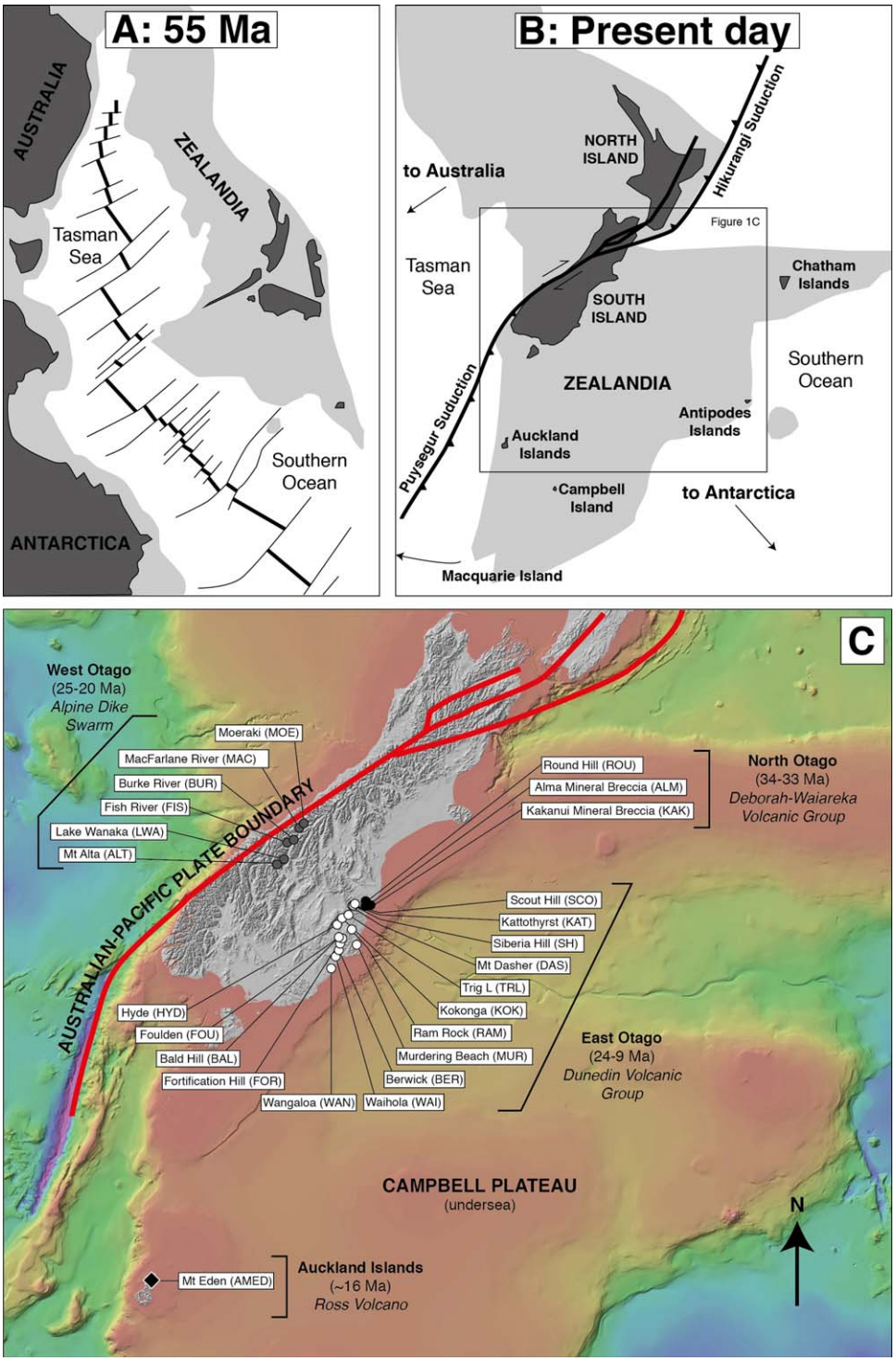

Figure 1. (a) Reconstruction of the paleo-Pacific Gondwana margin at ~55 Ma, with approximate positions of the present-day exposed crustal segments shown in dark gray, undersea crust in pale gray, and oceanic crust in white. This diagram is constructed for the time before the Australia-Pacific plate boundary propagated through the centre of Zealandia. Modified from *Mortimer et al*. [2012]. (b) Present-day map of Zealandia showing portions of continental crust above sea level (dark gray) and portions below sea level (light gray), as well as oceanic crust (white), and the Australia-Pacific plate boundary (prominent fault line that traverses through Zealandia). (c) Peridotite locations discussed in the text and plotted on a bathymetric map (source: NIWA). The letter code after each location indicates the prefix to samples collected from that site.

oceanic basalts [e.g., *Hart*, 1984; *Zindler and Hart*, 1986; *Hofmann*, 2003; *Stracke et al*., 2005] and its origin is typically attributed to recycling of ancient altered oceanic crust [e.g., *Chase*, 1981; *Hofmann and White*, 1982; *Stracke et al*., 2003; *Nebel et al*., 2013]. The origin of the HIMU signature in the Zealandia intraplate basalts, however, remains a contentious topic, with debate as to whether it is derived from an asthenospheric or lithospheric source. The term "HIMU-like" is used herein because the isotopic signatures of the Zealandia intraplate basalts do not completely overlap with the HIMU isotopic fields, and there is no known link with oceanic crust recycled in a plume [*Timm et al*., 2010].

Arguments for a lithospheric mantle source for the Zealandia intraplate basalts are based upon contemporaneous HIMU-like magmatism also having occurred in the formerly contiguous continental areas of Antarctica [*Rocholl et al*., 1995; *Hart et al*., 1997; *Panter et al*., 2000; *Rocchi et al*., 2002; *Martin et al*., 2013], East Australia and Tasmania [*Lanyon et al*., 1993; *Zhang et al*., 2001; *Nasir et al*., 2010] but not the intervening ocean basins. The source region is suggested to have been a mantle lithospheric domain that was located under Gondwana and has since been dismembered during separation of the Australia-Zealandia-Antarctica Gondwana margin at ~85 Ma [*Panter et al*., 2006]. This interpretation is complicated by the discovery of dredged oceanic volcanic rocks with Sr, Nd, and Pb isotope ratios that hint at a HIMU-like component in their mantle source regions [*Mortimer et al*., 2012; *Kipf et al*., 2013]. *Kipf et al*. [2013] explain the occurrence of the oceanic HIMU-like signatures in the basalts as being derived from continental lithosphere that was translated out from beneath continental West Antarctica and then partially melted beneath adjacent oceanic crust. As an alternative to a lithospheric source, *Hoernle et al*. [2006] and *Timm et al*. [2009, 2010] have argued that the basaltic HIMU-like signature originates from a large reservoir located deep (~600 km) in the asthenosphere, and that the lithosphere has played only a minor, if any, role.

It is the volcanoes of Zealandia that contain the strongest HIMU-like source signatures of all the SW Pacific continental intraplate magmas. Determining the composition of the Zealandia SCLM must be a first step in assessing the role of the lithosphere in these intraplate basalts. Prior to our study, the Zealandia SCLM was assumed to have relatively radiogenic Sr ($^{87}Sr/^{86}Sr > 0.7035$) and unradiogenic Nd ($^{143}Nd/^{144}Nd < 0.5128$) and Pb ($^{206}Pb/^{204}Pb = 18.7–18.9$) isotopic compositions [e.g., *Hoernle et al*., 2006; *Timm et al*., 2010; *McGee et al*., 2013]. Although such compositions would appear to rule out the SCLM having a HIMU-like component, these values are an "expected composition" based upon dredged schists and granites, Cretaceous subduction-related volcanoes that have reacted with continental crust, and dikes in Antarctica [*Hoernle et al*., 2006; *Timm et al*., 2010]. The isotopic composition of the Zealandia SCLM is thus effectively unknown.

The Zealandia Oligocene-Early Miocene intraplate basalts carry a cargo of mantle material [*Reay and Sipiera*, 1987; *Weaver and Smith*, 1989] that provides a direct opportunity of establishing the composition of the underlying SCLM. In the course of this study, hundreds of peridotite xenoliths have been collected from Oligocene-Miocene volcanic rocks across southern New Zealand with a twofold aim. First, 157 of these peridotites are used to generate the first regional compositional (petrography, major elements, trace elements) and isotopic (Sr-Nd-Pb-Hf) description of the Zealandia SCLM. These data highlight the unexpected occurrence of adjacent moderately fertile and highly refractory domains, both variably overprinted by LREE-enriched metasomatism. Second, with regional context in place, we then critically assess the role that the SCLM may have played in producing the HIMU-like source signature seen in the intraplate basalts.

2. Geological Setting

Zealandia is an amalgam of crustal tectonostratigraphic terranes that were accreted to the Gondwana convergent margin [*Landis and Coombs*, 1967; *Bradshaw*, 1989; *Mortimer*, 2004; *Cooper and Ireland*, 2013]. The oldest known rocks are Cambrian sediments and volcanic rocks [*Münker and Cooper*, 1999]. However, the majority of the accreted crustal fragments are metamorphosed Paleozoic to Mesozoic sediments that were deposited on oceanic lithosphere, or relatively immature arcs that were also built on oceanic lithosphere [*Mortimer*, 2004, and references therein]. No Proterozoic or older continental crust has been identified. At ~110 Ma, the paleo-Pacific Gondwana margin began to undergo extension [*Gibson et al*., 1988; *Tulloch and Kimbrough*, 1989; *Waight et al*., 1998a; *Scott and Cooper*, 2006; *Tulloch et al*., 2009b]. This led to fragmentation of Zealandia from Australia and Antarctica by ~85 Ma and the formation of intervening oceanic basins now represented by the Tasman Sea and the Southern Ocean [*Gaina et al*., 1998; *Tulloch and Kimbrough*, 1989; *Waight et al*., 1998b; *van der Meer et al*., 2013] (Figure 1b). Sea floor spreading has transported

Zealandia about 3500 km northward of its Cretaceous geographic position [*Bradshaw*, 1989]. While the geology and history of Zealandia's continental crust is well characterized, peridotite xenoliths provide insights in the nature and history of the underlying SCLM.

3. Peridotite Characterization

Previous investigation of Zealandia peridotitic xenoliths has been at reconnaissance level at best. Brief petrographic descriptions and/or mineral chemistries have been reported by *Brown* [1954], *Wright* [1967], *Wallace* [1975], *Price and Wallace* [1976], *Reay and Sipiera* [1987], *Brodie and Cooper* [1989], *Tulloch and Nathan* [1990], *Sewell et al*. [1993], *Hoke et al*. [2000], *Duclos et al*. [2005], *McCoy-West et al*. [2013], and *Scott et al*. [2014]. He isotopes were reported for 10 samples [*Hoke et al*., 2000] and *Duclos et al*. [2005] reported seismic anisotropy measurements on eight of those specimens. Whole rock Os isotopes for 27 xenoliths, entrained from the Late Cretaceous to the Miocene, have been interpreted to show that parts of the Zealandia lithosphere underwent depletion at ~2 Ga [*McCoy-West et al*., 2013]. *Scott et al*. [2014] provided a description of the petrographic characteristics, major and trace element data for 23 xenoliths from a tight cluster of volcanoes in East Otago within the South Island, and suggested that these record carbonatite metasomatism.

The peridotite xenoliths reported in this paper (n = 157) are from 25 locations across southern Zealand (Figure 1c and tabulated in supporting information Table 1), and are subdivided into four suites:

1. North Otago: from the ~34–33 Ma basaltic Deborah-Waiareka Volcanics;

2. West Otago: from the ~25–20 Ma carbonatitic-lamprophyric Alpine Dike Swarm;

3. East Otago: from the ~24–10 Ma basaltic Dunedin Volcanic Group; and

4. Auckland Islands: from the ~16 Ma basaltic Ross Volcano.

All samples are spinel peridotites; garnet has not been observed and plagioclase is present only in small melt patches that contain euhedral spinel, a secondary clinopyroxene and variably altered glass. Spinel classification follows *Carswell* [1980] and textural classification follows *Harte* [1977]. Each xenolith has had mineral major elements measured by wavelength dispersal spectrometry on electron microprobes at either the University of Potsdam (Germany) or the University of Otago (New Zealand). Elemental data are used to estimate temperatures of equilibration with the clinopyroxene-orthopyroxene geothermometer calibration of Taylor [1998]. Due to the lack of a reliable geobarometer for spinel peridotites, pressure was set at 10 and 20 kbar to correspond to the spinel facies in fertile mantle. Clinopyroxene and amphibole trace element concentrations were measured by laser ablation inductively coupled plasma mass spectrometry at the University of Otago on single grains either in situ or on grains from handpicked mineral separates (n = 79). Radiogenic isotopic (Rb-Sr and Sm-Nd (n = 35), Pb (n = 23), and Hf (n = 12)) compositions were measured by thermal ionization mass spectrometry at the University of Copenhagen (Denmark) (Sr, Nd, and Pb) and multicollector inductively coupled mass spectrometry in joint laboratories at the Universities of Köln and Bonn (Germany) (Hf) on a further subset of clinopyroxene separates. The choice of samples for isotopic analysis was largely governed by the trace element concentrations of the elements in question and the amounts of material available. Further details are presented in supporting information Tables 1 (sample summary), 2 (isotope summary), File 3 (methodology, data, additional information), and Table 4 (representative analyses).

3.1. East Otago

Ninety xenoliths have been analyzed from 15 locations in East Otago (Figure 1c). Xenoliths from four of these locations (Kattothyrst, Siberia Hill, Mt Dasher and Scout Hill) have already been described in detail and, although the data are included in Figure 3 and supporting information Table 1, the reader is referred to *Scott et al*. [2014] for specific petrological information regarding those samples. Most of the East Otago xenoliths occur within monogenetic lavas of the Waipiata Volcanics subgroup of the larger Dunedin Volcanic Group. The main shield volcano phase (Dunedin Volcano) did not carry much of a xenolith load to the surface, and the only analyzed rocks to date are those from the Murdering Beach location. Xenoliths reach up to 50 cm in diameter in rare cases (e.g., Trig L), but are more commonly $\leq$ ~10 cm in diameter. The sample suite has an array of compositions that vary from lherzolite through to dunite and wehrlite (Figure 2), although the latter lithology has only been found at Kattothyrst [*Scott et al*., 2014]. Textures vary from

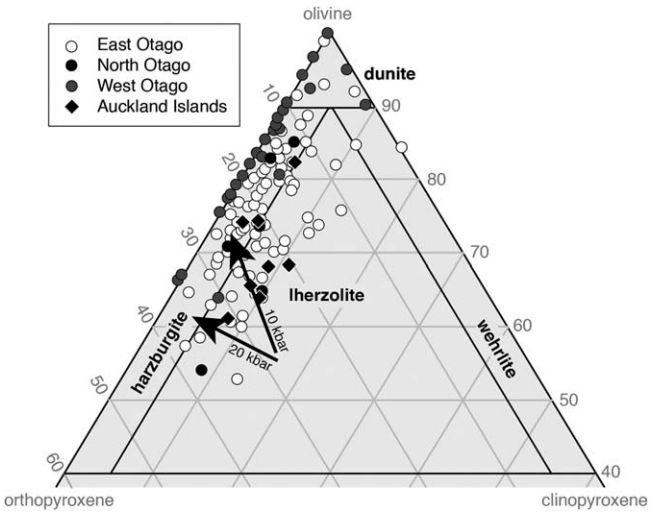

Figure 2. The ultramafic ternary diagram from *Streckeisen* [1976] illustrates the spread in modal compositions for the southern Zealandia xenolith suites. Modal percentages were calculated from 500 points per sample (see supporting information Table 1 for data). The 10 and 20 kbar melting paths are from *Niu et al.* [1997].

coarse-porphyroclastic to granuloblastic. Spinel grains are commonly distributed throughout the rocks. However, there are exceptions, such as those from Trig L, Murdering Beach, and Hyde, where the spinels occur in clusters that are associated with pyroxene. These textures resemble spinel-pyroxene symplectitic intergrowths after garnet [e.g., *Smith*, 1977; *Špaček et al*., 2013].

Average olivine Mg# (100*Mg/(Mg+Fe)) varies substantially across the East Otago suite, and subtle subgroups are distinguishable (Figure 3a). For example, the majority of xenoliths from Fortification Peak have olivine Mg# $>$ 91, whereas most xenoliths from Trig L have olivine Mg# $\leq$ 91 (Figures 3a–3c). Increasing olivine Mg# has a positive trend against increasing orthopyroxene Mg# and highlights a linear array (Figure 3a). Orthopyroxene Al_2O_3 contents generally decrease with higher olivine Mg# but the data are fairly dispersed (Figure 3c). Spinel Cr# (100*Cr/(Cr+Al)) also tends to rise with higher olivine Mg# (Figure 3b). The majority of East Otago spinels are Al-spinel. Kattothyrst, Siberia Hill, and Ram Rock spinels stand out from this broad pattern, being largely Cr-spinel and chromite and plotting at a higher Cr# for a given olivine Mg#. Clinopyroxene Al_2O_3 contents vary from 8.11 to 1.74 wt %, and this wide range can be found at a single location (e.g., Waihola subsuite). In this paper, we report maximum measured pyroxene Al_2O_3 values, which almost always correspond to the cores of grains (in some cases, the rims have up to 0.5 wt % less Al_2O_3 than the cores [*Scott et al*., 2014]). There is a good correlation between decreasing clinopyroxene Al_2O_3 and lower Na_2O or higher Mg# (not shown). Temperatures of equilibration for these spinel facies rocks vary between 710 and 1114°C (supporting information Table 1).

3.2. North Otago

Eleven peridotite xenoliths were analyzed from three North Otago locations: the Alma Mineral Breccia, the Kakanui Mineral Breccia, and a tuff at Round Hill (Figure 1c). The host rocks are all part of the middle Oligocene Deborah-Waiareka Volcanics [*Coombs et al*., 1986]. With the exception of peridotites from the Alma Mineral Breccia, which have had olivine and orthopyroxene completely altered to clay, the xenoliths are classified as lherzolite and harzburgite (Figure 2). The rocks display coarse-equant to coarse-porphyroclastic textures. Spinel grains are commonly distributed throughout the specimens with the exceptions of KAK-4 and ROU-1, where they form clusters that are associated with clinopyroxene and orthopyroxene. Amphibole-bearing clinopyroxenite veins cut across several Kakanui Mineral Breccia spinel peridotites. North Otago olivine Mg# shows little variation (89.3 and 90.9). Spinel Cr# for the Round Hill peridotites (8.8–12.4) overlaps with those from the Alma Mineral Breccia (10.1–15.5), but both locations have lower spinel Cr# than the Kakanui Mineral Breccia peridotites (19.5–41.0). North Otago olivine Mg# and spinel Cr# overlaps olivine and spinel in the East Otago suite (Figure 3b). Clinopyroxene and orthopyroxene compositions also vary between North Otago locations. The majority of the North Otago samples have maximum clinopyroxene Al_2O_3 contents of $>$ 6.5 wt % and orthopyroxene Al_2O_3 contents of $>$ 4.8 wt% (Figure 3c). Kak-3 and Kak-4, however, have distinctly lower Al_2O_3 in orthopyroxene ($<$ 3.11 wt%) and clinopyroxene ($<$ 5.55 wt %). There is a correlation between lower pyroxene Al_2O_3 and increasing spinel Cr#. KAK-2 contains a green-yellow pargasitic amphibole that appears to be partially replacing clinopyroxene. Temperatures of equilibration fall between 715 and 921°C (supporting information Table 1).

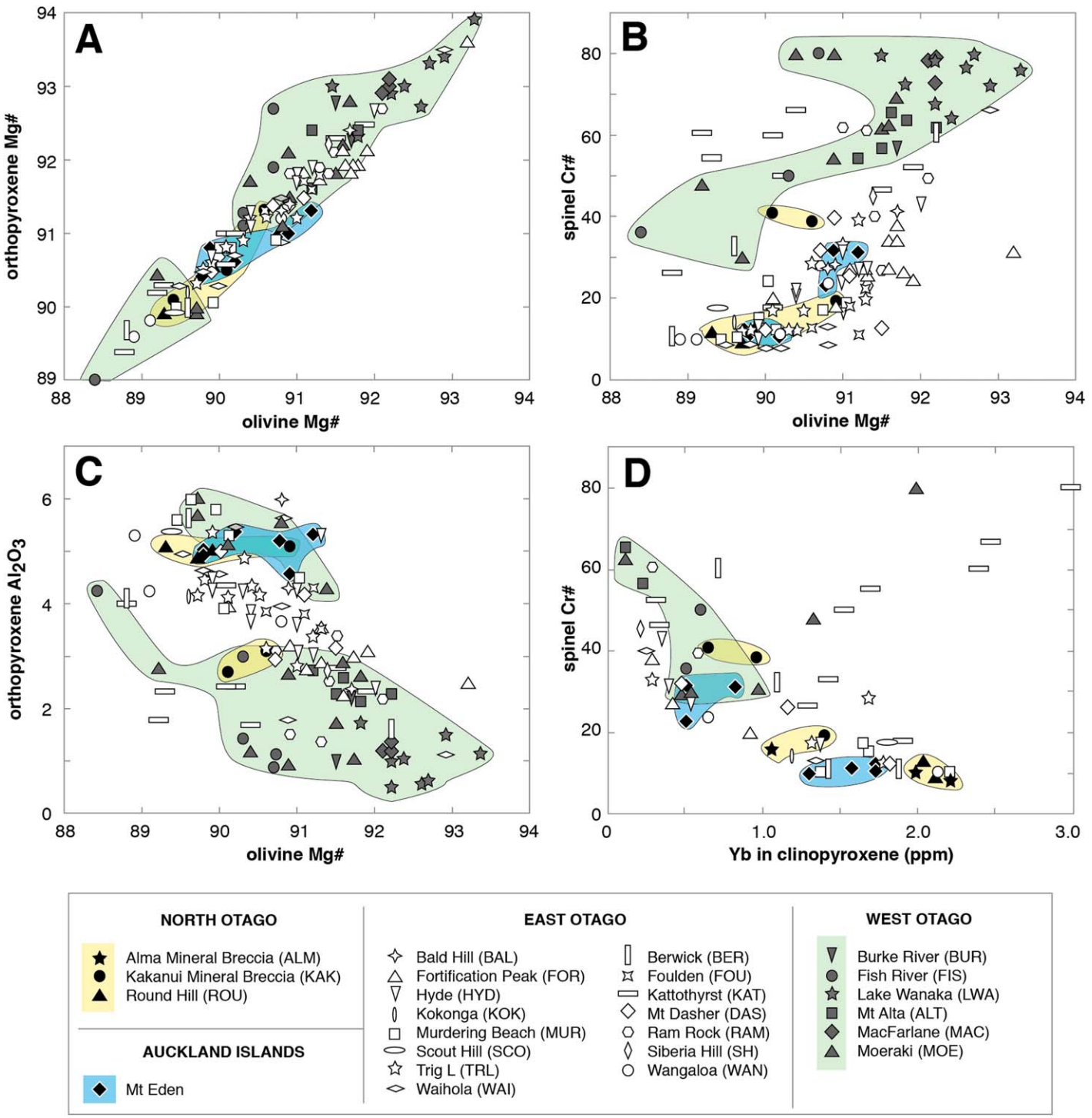

Figure 3. (a–d) Peridotite mineral chemistries illustrate the similarities and differences between the studied peridotite suites. Mg# and Cr# are the averaged values for each sample; Al_2O_3 is the maximum measured content. Relevant mineral data discussed in the text are tabulated in supporting information Table 1.

3.3. West Otago

Forty-nine xenoliths have been analyzed from diatremes at Mt Alta, Lake Wanaka, and Moeraki River; dikes in the Burke River and Fish River; and a dike boulder found in MacFarlane River (Figure 1c). The host rocks are part of the ~25–20 Ma carbonatitic-lamprophyric Alpine Dike Swarm [*Cooper*, 1986; *Cooper et al*., 1987; *Cooper and Paterson*, 2008], which overlaps with the earliest portions of the Dunedin Volcanic Group. Peridotite xenolith diameters rarely exceed 20 cm, and are mostly about 5 cm in diameter. Textures are

commonly coarse-equant and coarse-porphyroclastic, although mylonitic fabrics in which olivine grains have recrystallized to a very fine grain size occur in several specimens from the Lake Wanaka and Moeraki River diatremes.

The West Otago peridotite suite displays a number of notable petrographic features. First, clinopyroxene is rare or absent and the modal compositions are dominantly harzburgite or dunite (Figure 2). Lherzolite has only been found in the Moeraki River diatreme. Second, several peridotites from each West Otago location contain well-developed spinel-orthopyroxene ± clinopyroxene symplectites (see also Figure 1 of *Wallace* [1975]). These textures are significantly better developed than the symplectites observed in some East Otago peridotites. Third, hydrous minerals occur in several xenoliths each from the Fish River, Burke River, and Lake Wanaka locations. The majority of West Otago peridotites have olivine Mg# between 90 and 93 (Figure 3a). However, Mg# in olivine in several Fish River peridotites extends to as low as 84.8, with the lowest values correlating with grains adjacent to amphibole/phlogopite ± clinopyroxene, titanomagnetite, and apatite-bearing veinlets. Samples from the Lake Wanaka diatreme have the highest olivine Mg# (mostly > 92). A prominent chemical feature of the West Otago suite is that orthopyroxene Al_2O_3 contents are mostly less than 3 wt % and in some cases less than 1 wt % (Figure 3c). The low orthopyroxene Al_2O_3 in part stems from the occurrence of abundant minute exsolved rods of spinel that were too fine to analyze by microprobe. However, results from broad-beam analysis suggest that reintegration of spinel and orthopyroxene would be unlikely to significantly raise the orthopyroxene Al_2O_3 content. The high spinel Cr# of single grains occurring in the matrix through the peridotites shows a significant departure from those in East Otago, North Otago, and the Auckland Islands (Figure 3b). The spinels are Cr-spinel or chromite; no Al-spinel has been found, even in samples modally classified as lherzolite. Cr-amphibole and phlogopite occur in some Lake Wanaka, Fish River, and Burke River xenoliths where they form single grains or, rarely, veinlets. These hydrous minerals are associated with Cr-diopside, apatite, olivine ± titanomagnetite, and carbonate. The amphibole and phlogopite grains contain up to 3 and 2 wt % Cr_2O_3, respectively. Olivine Mg# tends to decrease toward these veinlets. The apatite grains are packed full of unidentified minute inclusions. Temperatures of equilibration fall between 830 and 1071°C (supporting information Table 1). Cr-rich peridotites can be free of garnet to pressures far greater than 20 kbar [*Robinson and Wood*, 1998; *Klemme*, 2004]; nevertheless, the calculated temperatures likely represent reasonable estimates because varying pressure by 10 kbar has only minor effect on temperature (~ 30°C).

3.4. Auckland Islands

Nine mantle xenoliths were recollected from a small plug on the northern part of the sub-Antarctic Auckland Islands first described by *Wright* [1967]. Most specimens from this location are greater than 10 cm in diameter, with the largest up to 40 cm in diameter. The xenoliths AMED-1, 2b, 7, 9, 12 are coarse-textured, AMED-3 contains porphyroclasts of clinopyroxene, olivine, and orthopyroxene, and AMED-4, 5, and 6 have spinel-pyroxene symplectites similar to those noted in East Otago. The Auckland Islands samples show the least chemical variation in southern Zealandia (Figure 3). Orthopyroxene has Mg# between 89.8 and 91.7 and maximum Al_2O_3 between 5.41 and 4.53 wt % (Figure 3c). Clinopyroxene Mg# in all samples varies between 89.0 and 92, and Al_2O_3 contents are between 5.35 and 7.21. There are, however, two subtle subgroups within this peridotite suite; the coarse-textured and porphyroclastic samples have olivine Mg# between 89.7 and 90.3, whereas the symplectite-bearing peridotites have slightly higher values (90.7–91.3) (supporting information Table 1). In the coarse-textured specimens, spinel has an Al-spinel composition (Cr# between 10 and 16), whereas in symplectite-bearing samples it is Al-spinel to Cr-spinel (Cr# between 22 and 31) (Figure 3b). The equilibration temperatures are distinct between the two textural groups of peridotite: the coarse-textured samples record temperatures of between 881 and 960°C, whereas the symplectite-bearing samples equilibrated between 1078 and 1259°C (supporting information Table 1).

4. Trace Elements

Trace element concentrations provide detailed information on the degree of SCLM depletion and/or enrichment [e.g., *Eggins et al*., 1998; *Downes*, 2001; *Pearson et al*., 2003]. Clinopyroxene is the principal repository of trace elements in the peridotites examined, with exceptions of amphibole in several of the West Otago samples and three North Otago samples, and apatite in several East Otago and West Otago samples. Average normalized trace element values are illustrated in Figures 4–7. Trace element plots with all analyses are presented in supporting information Table 4.

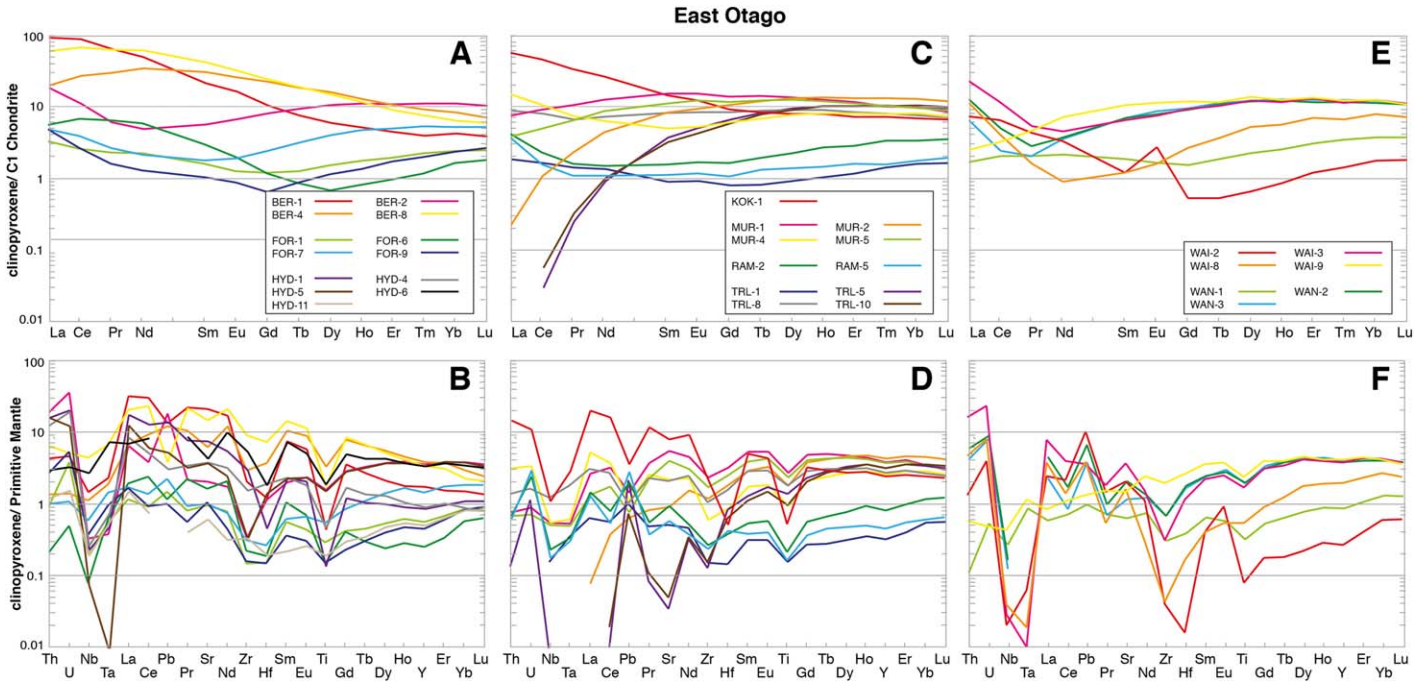

Figure 4. Averaged clinopyroxene trace element patterns for East Otago peridotites normalized to C1 Chondrite (a, c, and e) and Primitive Mantle (b, d, and f) values of *Sun and McDonough* [1989]. Sample locations are shown alphabetically. Plots of individual clinopyroxene analyses can be found in supporting information File 3, and representative data in supporting information Table 4. Gaps in the data represent elements below LA-ICP-MS detection limits.

4.1. East Otago

East Otago clinopyroxene shows a complete spectrum of trace element patterns. Many samples show evidence for having undergone high levels of melt extraction, as indicated by HREE concentrations of $<$ 10 times Chondrite (Figures 4a, 4c, and 4e). Most of these samples also display the distinctive signs of having experienced metasomatic addition of LREE, as illustrated by upward inflections in normalized LREE (e.g., Figures 4a–4f). The spoon-shaped Chondrite normalized patterns also point to addition of LREE to rocks already highly depleted. Samples with lower HREE concentrations tend to be those that have high olivine Mg# and spinel Cr#. Chondrite-normalized plots show that several samples have HREE equal to $\sim$10 times Chondrite but are relatively depleted in LREE (e.g., Figure 4c). Such profiles are indicative of low-moderate degrees of melt extraction. Many samples display distinct Primitive Mantle-normalized Nb, Zr, Hf, and Ti negative anomalies (Figures 4b, 4d, and 4f). WAI-2 has a positive Eu anomaly (Figure 4e) that could be explained if plagioclase was present at some stage and underwent preferential melt extraction (none occurs in the inspected sample now). This sample also has extreme depletions in Hf, Zr, and Nb (Figure 4f).

4.2. North Otago

There are some subtle differences between the clinopyroxene trace elements across the three North Otago locations. In the Alma Mineral Breccia, ALM-1 and ALM-4 have elevated LREE concentrations when compared with ALM-2 and ALM-3 (Figure 5a). ALM-1 also displays very prominent Primitive Mantle-normalized Ti, Zr, and Hf negative anomalies. When compared with KAK-1 and KAK-2, sample KAK-3 and KAK-4 have lower HREE concentrations as well as larger negative Primitive Mantle-normalized Nb, Ti, Zr, and Hf anomalies (Figure 5b). ROU-1 and ROU-3 are distinct from those from the Kakanui Mineral Breccia and Alma Mineral Breccia because they show LREE depletion trends. ROU-2 has a similar HREE-normalized content to ROU-1 and ROU-3 but displays a variable LREE enrichment pattern indicating LREE inhomogeneity within clinopyroxene.

4.3. West Otago

Clinopyroxene trace elements in the West Otago suite display striking LREE-enrichment patterns. All samples have sinusoidal Chondrite-normalized trends made up of low HREE concentrations relative to MREE and/or LREE (Figure 5c). Two samples from the Mt Alta diatreme (ALT-4, ALT-7) have the highest

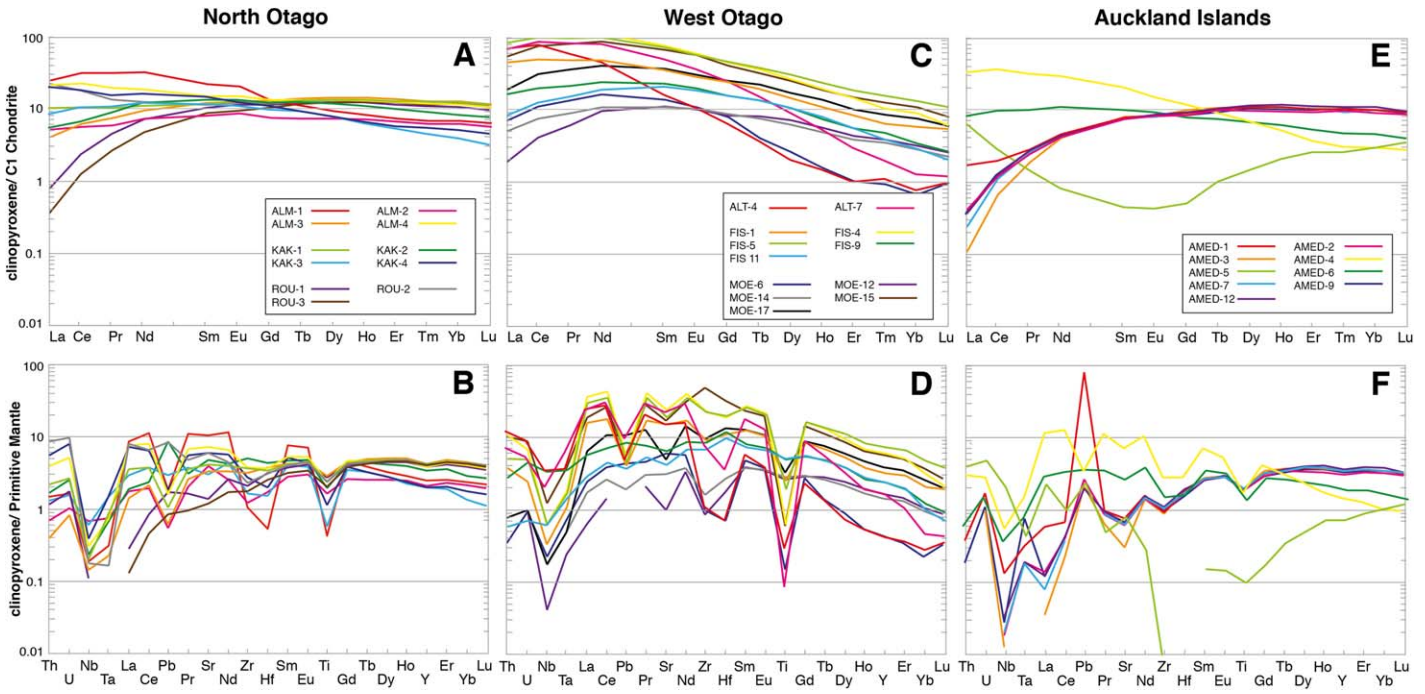

Figure 5. Averaged clinopyroxene trace element patterns for North Otago (a and b), West Otago (c and d), and the Auckland Islands (e and f). Clinopyroxene averages are normalized to C1 Chondrite or Primitive Mantle values of *Sun and McDonough* [1989]. Plots of individual clinopyroxene analyses can be found in the supporting information File 3, and representative data in supporting information Table 4. Gaps in the data represent elements below LA-ICP-MS detection limits.

clinopyroxene LREE/HREE profiles in the entire trace element suite. Most clinopyroxene grains also show very prominent Nb, Pb, and Ti negative anomalies (Figure 5d). Clinopyroxene Sr, Zr, and Hf negative anomalies are also present in some samples, with exceptions being MOE-15 and MOE-17 which have positive or no Zr $\pm$ Hf anomalies.

4.4. Auckland Islands

The high and low temperature samples from this location have distinct trace element profiles. Clinopyroxene grains in the coarse and porphyroclastic low-T suite overlap one another, with HREE concentrations around 10 times Chondrite but low LREE (Figure 5e). In contrast, the symplectite-bearing high-T samples have low HREE contents and upward inflections in LREE (Figure 5e). AMED-5 is particularly notable for its extreme depletion in MREE. Primitive Mantle-normalized diagrams further illustrate differences in HREE and LREE concentrations between samples (Figure 5f).

5. Radiogenic Isotopes

To assess the isotopic composition of the enrichment agents and to place broad constraints on the timing of depletion and metasomatism, clinopyroxene grains have been separated and Sr-Nd-Pb-Hf isotopes measured. Data are tabulated in supporting information Table 2 and the methodology discussed in supporting information file 4. Sr, Nd, and Hf isotope data are corrected to the age of eruption, with differences between measured and age-corrected values generally less than or close to reproducibility and trivial compared to the spread in the data set. The clinopyroxene separates yield a spread of Sr and Nd isotope compositions with $^{87}Sr/^{86}Sr_i$ between 0.70169 and 0.70351 and $^{143}Nd/^{144}Nd_i$ between 0.51263 and 0.51372 ($\varepsilon Nd_i = +0.3$ to $+21.5$) (supporting information Table 2). These isotope ratios broadly overlap with the MORB field (Figure 6a), although many samples plot at lower εNd_i for a given $^{87}Sr/^{86}Sr_i$. The isotope ratios overlap with the unradiogenic end of the intraplate basalt Sr isotope spectrum but extend to even less radiogenic compositions. Some samples (TRL-10, MUR-2) have radiogenic Nd and/or unradiogenic Sr isotope compositions that indicate considerably greater time-integrated depletion than typical for MORB or OIB mantle sources.

Clinopyroxene Pb isotope ratios extend to realms more radiogenic than MORB (Figures 6b–6d) with $^{206}Pb/^{204}Pb = 19.03–21.41$, $^{207}Pb/^{204}Pb = 15.60–15.77$, and $^{208}Pb/^{204}Pb = 38.58–40.75$. One sample (KAK-2)

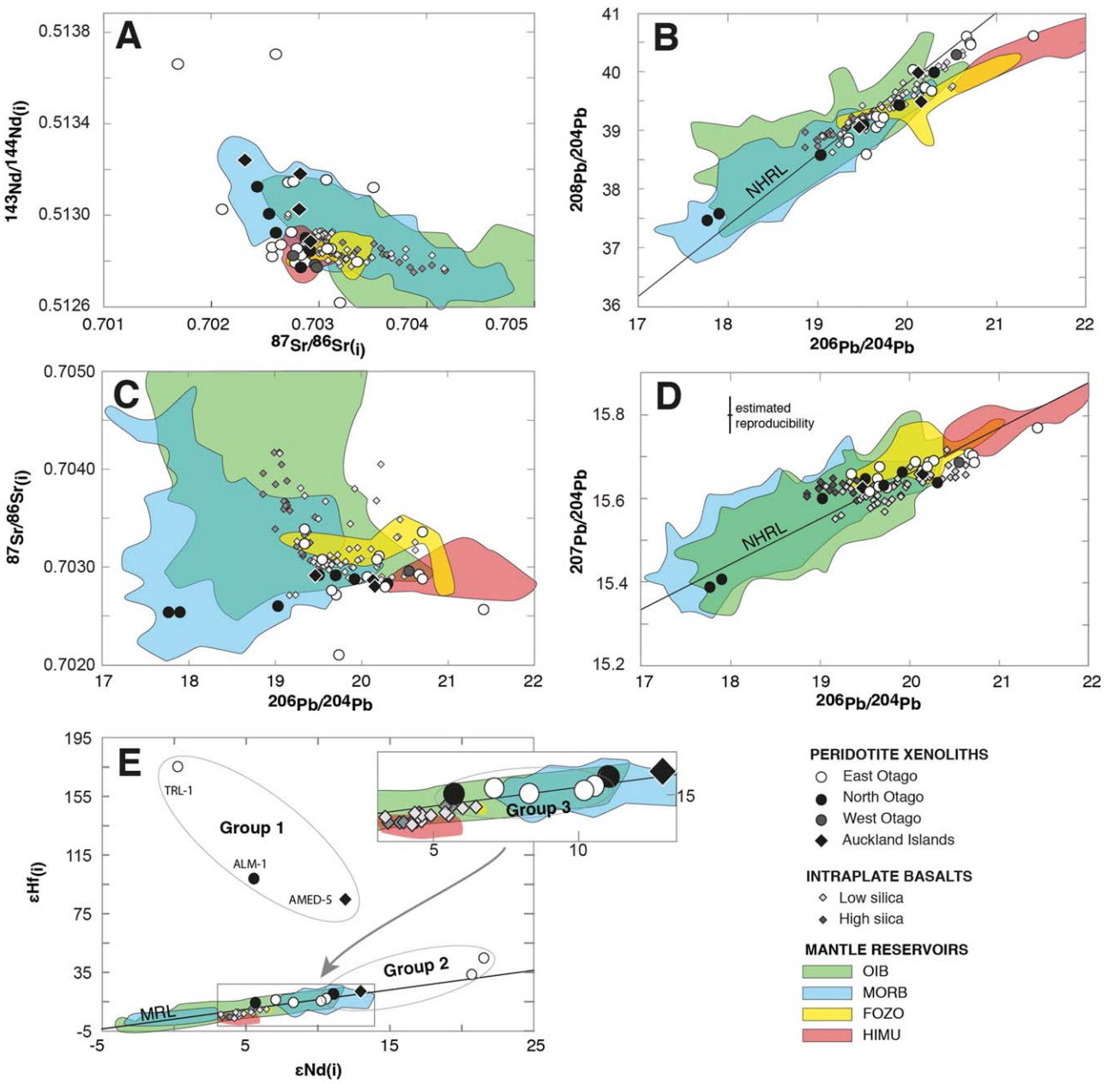

Figure 6. Selected isotope plots for Zealandia peridotites (clinopyroxene; this study) and Zealandia intraplate basalts (whole rock; from the compilation of *Timm et al*. [2010]). (a) $^{143}Nd/^{144}Nd_i$ versus $^{87}Sr/^{86}Sr_i$ in peridotites and basalts, compared with the mantle reservoirs of *Stracke et al*. [2003]. (b) $^{208}Pb/^{204}Pb$ versus $^{206}Pb/^{204}Pb$ plot with NHRL (Northern Hemisphere Reference Line) from *Hart* [1984]. (c) $^{87}Sr/^{86}Sr_i$ versus $^{206}Pb/^{204}Pb$. Note the apparent divergence in intraplate basalt and peridotite trends. (d) $^{207}Pb/^{204}Pb$ versus $^{206}Pb/^{204}Pb$ plot. (e) εNd versus εHf with enlarged inset of the data falling close to the MRL (mantle reference line from *Vervoort et al*. [1999]). Groups 1, 2, and 3 are distinguished on the basis of Hf-Nd isotope and REE systematics (see text for further discussion). See supporting information Table 4 for analytical methods and discussion of age corrections.

has a distinctly less radiogenic composition at $^{206}Pb/^{204}Pb = 17.90$, $^{207}Pb/^{204}Pb = 15.41$, and $^{208}Pb/^{204}Pb = 37.58$; a duplicate analysis ran poorly but yielded similar values. Most samples show Pb isotope variations that mimic those observed in the intraplate basalts by tending to plot close to and cross-cut the Northern Hemisphere Reference Line (NHRL). More radiogenic samples plot beneath the NHRL and less radiogenic samples above it in both $^{208}Pb/^{204}Pb$–$^{206}Pb/^{204}Pb$ and $^{207}Pb/^{204}Pb$–$^{206}Pb/^{204}Pb$ space (Figures 6b and 6d). The $^{206}Pb/^{204}Pb$ ratios are close to the composition of the FOZO and HIMU mantle reservoirs defined by *Stracke et al*. [2003] and overlap with intraplate Zealandia basalt compositions. However, $^{208}Pb/^{204}Pb$ ratios tend to be more radiogenic and $^{207}Pb/^{204}Pb$ less radiogenic than the HIMU field defined by *Stracke et al*. [2003].

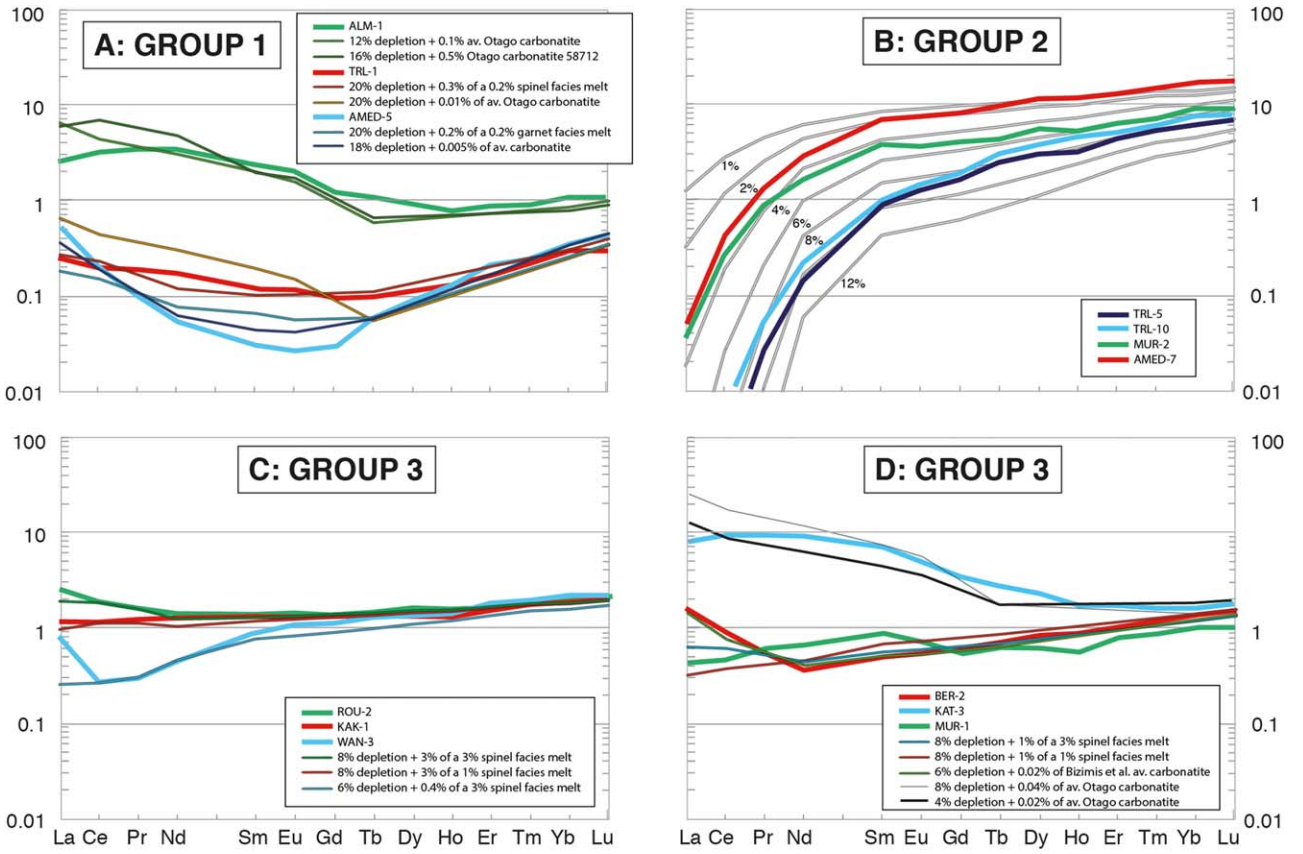

Figure 7. (a–d) Depletion and enrichment models for theoretical equilibrium whole rock compositions calculated using measured clinopyroxene REE and modal abundances. Samples are divided into Groups 1–3 on the basis of combined REE and Hf and Nd isotopic compositions (see Figure 6e and text). The variably depleted mantle source is assumed to have had an originally depleted mantle composition [*Salters and Stracke*, 2004] and metasomatizing agents include low-degree silicate melts or carbonatitic compositions from *Bizimis et al.* [2003a] and *Cooper and Paterson* [2008]. All diagrams normalized to C1 Chondrite of *Sun and McDonough* [1989]. Further details of the modeling and parameters are given in supporting information File 5.

Clinopyroxene Hf isotope concentrations vary between $^{176}Hf/^{177}Hf_i = 0.28310$ and 0.28771 ($\varepsilon Hf_i = +12$ to $+175$). Most samples plot along the mantle reference line of *Vervoort et al.* [1999] and either overlap with the MORB field or extend to more radiogenic compositions (Figure 6e). TRL-1, ALM-1, and AMED-5 have extremely radiogenic Hf compositions that plot well above the mantle array. The Hf isotope values are distinct from HIMU, which has relatively unradiogenic $^{176}Hf/^{177}Hf$ compared to MORB [*Stracke et al.*, 2005; *Nebel et al.*, 2013].

6. Coupled REE-Isotope Modeling

To examine the origin and evolution of the peridotites, an attempt is made to model the clinopyroxene REE and isotope data. Following similar investigations [e.g., *Stracke et al.*, 2011; *Liu et al.*, 2012], trace element modeling is restricted to the REE and Hf-Nd isotopes because these are the most informative with respect to depletion-enrichment histories. Insufficient sample material was available to enable Hf isotopic analysis of clinopyroxene from West Otago, so by necessity we focus upon the East Otago-North Otago-Auckland Islands data set. Our method of the isotope-trace element modeling is summarized in supporting information File 5.

REE were modeled by adding various metasomatic components to variably depleted residues by bulk mixing (Figure 7). The effects of depletion and metasomatism are most evident in the LREE because these elements are preferentially removed during melt depletion and common metasomatizing agents are LREE enriched. HREE concentrations are less affected by metasomatism and can be used as proxies for melt depletion. The choice of metasomatizing agent has important implications. Previous modeling attempts for

enrichment of depleted peridotite have used low-degree silicate melts as the metasomatic agent [e.g., *Stracke et al*., 2011; *Liu et al*., 2012]. However, carbonatitic melts have been inferred to have reacted with SCLM in many off-craton locations including Africa [e.g., *Dautria et al*., 1992; *Rudnick et al*., 1993; *Wittig et al*., 2010], Antarctica [e.g., *Martin et al*., 2013], Arabia [e.g., *Shaw et al*., 2007], Australia [e.g., *Yaxley et al*., 1998; *O'Reilly and Griffin*, 2000], Europe [e.g., *Ionov et al*., 1993; *Witt-Eickschen et al*., 2003], and New Zealand [*Scott et al*., 2014]. Our modeled carbonatitic compositions come from carbonatitic dikes that occur in West Otago [*Cooper and Paterson*, 2008] and a published average carbonatitic composition from *Bizimis et al*. [2003a]. To compare our data with the REE depletion-metasomatism models, the clinopyroxene REE are converted to equilibrium whole rock compositions using modal data.

Following *Stracke et al*. [2011] and *Liu et al*. [2012], two end-member scenarios are considered (Figure 8). The first infers ancient melt-rock interaction, where depletion occurs at some point in the past and is followed immediately by metasomatism with the resultant rock then evolving undisturbed to the present. The second scenario also involves source depletion in the past, but metasomatism occurs at the modern day immediately prior to xenolith entrainment. Innumerable intermediate scenarios are possible and the isotopic consequences of some of these are discussed in supporting information File 5. In the case of Zealandia, Re-depletion ages for xenoliths range from 2.3 to 0.36 Ga [*McCoy-West et al*., 2013]. Because the oldest Zealandia continental crust is ~550–500 Ma, depletion is modeled at 2.0, 1.5, 1.0, and 0.5 Ga to encompass the potential for varying depletion events across the region.

Sequentially decreasing degrees of incompatibility of Nd, Hf, Sm, and Lu during mantle partial melting produce residues with a significantly greater increase in Lu/Hf than Sm/Nd. Ancient depletion followed by isolation and ingrowth will result in depleted lithologies with present day isotopic compositions significantly more radiogenic than modern depleted mantle. Low-degree silicate melts are enriched in REE and Hf compared to depleted mantle residues, and small amounts of metasomatism will result in relatively large changes in parent-daughter ratios and thus modern isotopic compositions that diverge significantly from (and are decoupled from) depleted mantle values. Addition of a small degree silicate melt with "normal" Sm/Nd and Lu/Hf to ancient depleted residues and subsequent ingrowth results in present day Hf and Nd isotopic compositions that are decoupled from typical modern mantle compositions, producing more radiogenic Hf at a given Nd isotope composition (Figures 8a and 8b; and *Liu et al*. [2012], *Stracke et al*. [2011], and *Pearson and Wittig* [2014]). Use of carbonatite as a metasomatic agent has an even more extreme effect on ancient mantle compositions due to its typically subchondritic Sm/Nd, higher Nd, and suprachondritic Lu/Hf [*Bizimis et al*., 2003a]. Even small degrees of ancient carbonatitic enrichment to a slightly depleted mantle source results in the trace element budget being dominated by the LREE of the carbonatitic component. The consequence is development of negative modern day εNd that is controlled by evolution of the metasomatic component, whereas the Hf isotopic evolution more closely follows that of the depleted residue and has radiogenic εHf (Figure 8c). Modern carbonatitic enrichment of ancient depleted residues results in εNd that is dominated by the metasomatizing composition and Hf isotope compositions that are decoupled and highly radiogenic; the resulting trends (Figure 8d) are very different from those generated by metasomatism by a low-degree silicate melt. Metasomatism of ancient depleted residues with either silicate or carbonatitic components can thus decouple Nd and Hf isotopes, with the magnitude of the decoupling dependent upon the composition of the metasomatizing agent and the relative timing of depletion and enrichment (Figures 8e and 8f).

The modeling process is an open-ended exercise and does not provide an exact solution for the origin and evolution of the observed REE patterns and isotope ratios. However, our goal is to use the results to demonstrate that the measured REE concentrations and isotope compositions are broadly consistent with processes of melt depletion and metasomatism and to allow estimation of the amounts of the metasomatic agent required. Combining the clinopyroxene REE systematics and Hf and Nd isotopic compositions permits identification of three groups (**Groups 1–3**) in the data set (Figure 7).

6.1. Group 1

Group 1 peridotites (TRL-1, ALM-1, AMED-5) have highly radiogenic εHf decoupled from typical mantle values (Figure 6e), and are characterized by spoon-shaped REE patterns and relatively low HREE (Figure 7a). In general, REE modeling indicates that the REE characteristics of the Group 1 samples are consistent with a highly depleted (16–20%) spinel facies depleted mantle that has undergone addition of small amounts ($<$0.5%) of LREE-enrichment (Figure 7a).

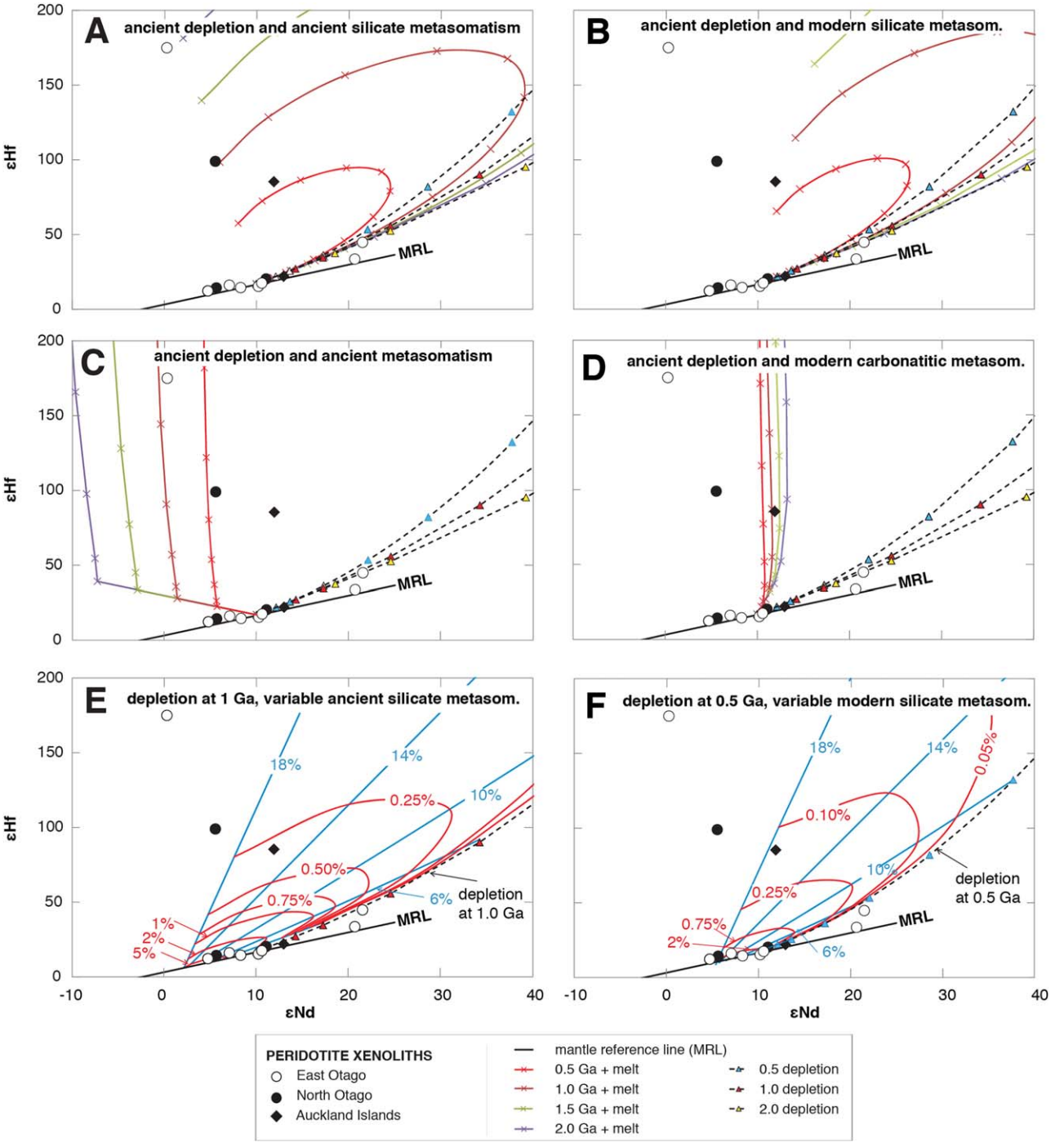

Figure 8. (a–f) Selected models illustrating the effects of ancient melt depletion and metasomatism on clinopyroxene Hf and Nd isotopic compositions. In Figure 8a dashed lines represent present day compositions of depleted mantle sources depleted by 1%, 2%, and then increments of 2% melting up to a maximum of 20% at 0.5, 1, and 2 Ga. Solid lines represent the effects of addition of a small amount (0.15%) of a metasomatic component to the variably depleted residual sources (1%, 2%, and then increments of 2% up to 20%) immediately after depletion, and then evolution to the present day. The silicate melt is a 0.2% melt of a deleted mantle source in the spinel field. Figure 8b as for Figure 8a but metasomatism is modern. In both models, the isotopic composition of the metasomatizing melt is assumed to be the same as the depleted source at the appropriate time. Figures 8c and 8d as for Figures 8a and 8b, respectively, but the metasomatizing agent is an average Otago carbonatite (from *Cooper and Paterson* [2008]). Figure 8e a model using the same parameters as Figure 8a illustrates the effect of increasing percentages of silicate metasomatizing component (red lines) to sources variably depleted at 1 Ga (blue lines), immediately after the depletion event. Figure 8f as for Figure 8e but source depletion occurred at 0.5 Ga, metasomatism is modern and the metasomatizing agent has trace element composition of a 0.2% melt in the spinel facies and the isotopic composition of an average low silica intraplate basalt. Analytical reproducibility for Hf and Nd isotopes is smaller than the symbol size. The mantle reference line in all diagrams is from *Vervoort et al.* [1999]. Full details of the model parameters are presented in supporting information File 5.

TRL-1 has the most extreme and decoupled isotopic composition in the data set with εHf = +175 and εNd = 0 (Figure 6e). The REE of this sample can be modeled by high degrees of melt depletion (20%) followed by addition of small amounts of either silicate melt (0.2–0.3% of a low-degree melt from spinel or garnet facies) or very small amounts (0.01%) of average carbonatite (Figure 7a). Such extreme decoupling of Hf from Nd has also been observed in some oceanic mantle samples [e.g., *Salters and Zindler*, 1995; *Bizimis et al*., 2003b; *Stracke et al*., 2011] and some on-craton and off-craton peridotites (see compilation in *Pearson and Wittig* [2014]). Our modeling shows that TRL-1 has Hf and Nd isotope compositions consistent with high degrees of ancient source depletion ($\sim$2 Ga), followed immediately by small degrees of metasomatism by a low degree melt (Figure 8a). This sample also comes from one of the localities where Os isotope data imply a depletion event occurred at $\sim$2 Ga [*McCoy-West et al*., 2013]. The isotopic composition of TRL-1 cannot be explained by ancient depletion followed by recent metasomatism (Figures 8b, 8d, 8f, and 8h) unless the metasomatizing component had a relatively unradiogenic isotopic composition (i.e., εHf and εNd of ca. 0), the consequences of which are to shift the modeled evolution curves toward lower εNd. No indication of such a source component has been encountered in any Zealandia rock.

Addition of a carbonatitic component to an ancient depleted source (e.g., Figures 7a, 8c, and 8d) is broadly consistent with the isotopic compositions of ALM-1 and AMED-5 but requires generally younger depletion events and lower degrees of depletion (8% at 1 Ga and 12% at 0.5 Ga) than suggested by the REE modeling (Figure 7a). However, the heterogeneous nature of carbonatites and their high incompatible trace element concentrations mean that these models are sensitive to the composition of the metasomatic end-member chosen. The Hf-Nd isotope composition of AMED-5, for example, can be modeled by either recent addition of a very small amount of a carbonatitic component or by addition of a silicate melt at $\sim \leq$ 0.5 Ga to a highly depleted component.

6.2. Group 2

Group 2 peridotites (MUR-2, TRL-5, TRL-10, and AMED-7) have εHf and εNd values that fall on or close to the mantle reference line but are more radiogenic than MORB. These samples are also characterized by LREE-depleted compositions (Figure 7b). REE modeling indicates that these compositions could be consistent with removal of small to moderate degrees of melt (3–10%) in the spinel facies (Figure 7b) with no subsequent metasomatism. The Hf-Nd isotopic evolution curves of ancient depleted mantle sources in Figure 8 (dashed lines) show that depletion and subsequent isolation would result in present day compositions that are more radiogenic than typical mantle sources sampled by MORB and OIB. Samples AMED-7 and TRL-5 have Nd-Hf isotopic compositions that are effectively the same as DM today. If these rocks were formed 500 Ma by the degrees of depletion suggested by REE modeling, then they should now have much more radiogenic compositions (e.g., εNd = 29 and εHf = 80); therefore depletion most likely occurred more recently than this. Depleted mantle Nd model ages (AMED-7 = 0.2 Ga, TRL-5 = 0.03 Ga) are also consistent with relatively recent derivation from a DM source. On the other hand, TRL-10 and MUR-2 have Hf and Nd isotopic compositions that are more radiogenic than modern MORB and require longer-term depletion and isolation. Depleted mantle Nd model ages (TRL-10 = 0.2 Ga, MUR-2 = 0.65 Ga) suggest depletion in the Phanerozoic. Isolation of a mantle source depleted by 10% at 2 Ga would result in isotopic compositions much more extreme (εNd = 120, εHf = 480) than observed in these samples, which contrasts with Re-depletion ages on xenoliths from these same locations [*McCoy-West et al*., 2013].

6.3. Group 3

Group 3 peridotites (BER-2, KAK-1, MUR-1, ROU-2, KAT-3, and WAN-3) have εHf and εNd values that fall on the mantle reference line and overlap with typical MORB compositions, but are typically more radiogenic than the intraplate basalts (Figure 6e). These samples have relatively flat to spoon-shaped LREE-enriched patterns (Figures 7c and 7d). These samples could have undergone moderate degrees of depletion (6–8%) of a depleted mantle source, followed by variable and generally larger amounts of metasomatism than Group 1 (Figures 8c and 8d). High degrees of silicate melt enrichment would overprint the residual-depleted source compositions (Figures 8e and 8f), which means that it is not possible to distinguish between relatively recent depletion followed by metasomatism and eruption from ancient depletion with ancient or modern melt addition, although in general ancient depletion + ancient metasomatism requires larger degrees of metasomatism than younger depletion + modern metasomatism to bring compositions back onto the mantle reference line (Figures 8e and 8f). The models more closely replicate the isotopic composition of the peridotites when a

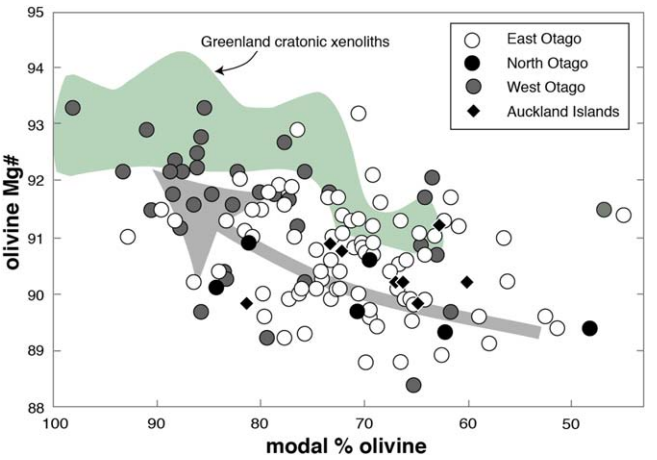

Figure 9. Olivine Mg# versus modal olivine diagram showing the variation in the four studied Zealandia peridotite suites. The gray arrow indicates the general melt depletion trend [*Boyd*, 1989], with data falling off this trend caused by enrichment processes. A number of the West Otago samples plot within the cratonic field for spinel facies depletion [*Bernstein et al*., 2007]. Olivine Mg# can be found in supporting information Table 1, as can the modal counts.

metasomatic component that is more enriched than depleted mantle is used (e.g., similar in composition to the intraplate basalts Figure 6). Carbonatitic enrichment is only consistent with the Group 3 isotopic compositions if depletion and metasomatism occurred relatively recently, such that there was insufficient time to allow for radiogenic ingrowth (models not shown). If source depletion was ancient (0.5 Ga or older), then small degrees of carbonatite metasomatism could result in Hf and Nd isotopic compositions that are offset from the mantle reference line similar to those observed in Group 1 (Figure 8d). BER-2, however, is only slightly enriched in LREE compared to a depleted residue and is best modeled by addition of a very small amount (0.02%) of a carbonatitic component to a moderately depleted residue (Figure 7d). Therefore, depletion and replenishment of this sample must have been relatively recent and there has been insufficient time for ingrowth to change the isotopic compositions.

7. Discussion

7.1. Adjacent Fertile and Refractory Domains Beneath Zealandia

Before we can address the role of the Zealandia SCLM in intraplate basalt genesis, we must synthesize its composition, as this has not been done before. The peridotite major and trace element data reveal the unexpected result that moderately fertile SCLM domains beneath East Otago, North Otago, and the Auckland Islands reside adjacent to a highly refractory domain beneath West Otago. The West Otago harzburgite-dunite modal compositions (Figure 2) are accompanied by Mg-rich olivine (Figure 3a), high spinel Cr# (Figure 3b), and low orthopyroxene Al_2O_3 (Figure 3c). The few West Otago xenolith clinopyroxenes that are available have distinctly low HREE and Ti, Zr, Nb, and Hf concentrations (Figures 3d and 5). The olivine Mg#, spinel Cr#, orthopyroxene Al_2O_3, and clinopyroxene HREE contents can be explained in terms of extensive melt extraction because Fe, Yb, and Al act incompatibly and Cr and Mg compatibly during spinel facies melting [*Dick and Bullen*, 1984; *Hellebrand et al*., 2001; *Lee et al*., 2001]. It is striking that the some West Otago olivine grains have Mg# that overlap spinel facies cratonic lithosphere (Figure 9). An olivine Mg# of 92.8 is the point at which partial melting should leave only a dunitic residue [*Bernstein et al*., 2007]. Many of the clinopyroxene ± orthopyroxene grains in the West Otago suite have therefore likely formed by metasomatic processes (discussed below).

Geothermometric results noted above and summarized in supporting information Table 1 indicate that the peridotite temperatures of equilibration for the four Zealandia suites fall between ~1260 and 710°C and cluster at ~ 900°C. Because Zealandia broke away from Gondwana at ~85 Ma [*Laird and Bradshaw*, 2004] and at the main time of xenolith entrainment (Late Oligocene to Early Miocene) had minimal topography [e.g., *Douglas*, 1986], there should have been little lateral mantle temperature variation beneath this continental mass. Therefore, the similar ranges of equilibration temperature imply that the depths of peridotite extraction between the different domains overlap. This is an important conclusion because it means that the broad compositional differences between the highly refractory West Otago and more fertile East Otago, North Otago and the Auckland Islands xenolith suites is most likely due to lateral SCLM variation. The geographical spread of the West Otago xenoliths indicates that this highly refractory craton-like domain extends for a minimum of 100 km in a northeast-southwest direction and is likely bisected at the northern

end by the Alpine Fault (Figure 1). An east-west width is unknown but, assuming equivalent mantle temperatures between East Otago and West Otago, one constraint is that it did not extend as far as East Otago only ~100 km to the east (Figure 1). Unlike some other situations where adjacent compositionally contrasting SCLM domains have been identified (e.g., India [*Griffin et al*., 2009a] or Spitsbergen [*Griffin et al*., 2012]), there is no obvious translithospheric suture separating the East and West Otago domains. In fact, the continental crust of Otago is dominated by Carboniferous and younger quartzofeldspathic metasedimentary rocks [*Turnbull*, 2000; *Forsyth et al*., 2006; *Rattenbury et al*., 2010; *Cooper and Ireland*, 2013]. Therefore, the West Otago lithosphere evidently has an early extensive depletion history that predates juxtaposition with the overlying continental crust.

The more fertile East Otago and North Otago SCLM domains also have early histories decoupled from the overlying continental crust. The ancient Hf depletion events identified in the North Otago and East Otago xenoliths (Figure 8) are consistent with Re-depletion model ages on other peridotite xenoliths from this area. *McCoy-West et al*. [2013] interpreted ancient Re-depletion ages as indicating the Zealandia SCLM represents a long-lived stable fragment of Palaeoproterozoic mantle. However, there is increasing evidence that the oceanic lithosphere can contain ancient Hf and Os isotopic compositions that represent portions of ancient lithosphere that have been preserved within convecting asthenosphere for long periods of time [e.g., *Parkinson et al*., 1998; *Brandon et al*., 2000; *Harvey et al*., 2006; *Bizimis et al*., 2007; *Liu et al*., 2008; *Simon et al*., 2008; *Dijkstra et al*., 2010; *Stracke et al*., 2011; *Rampone and Hofmann*, 2012; *Liu et al*., 2014]. As the Otago crustal lithosphere comprises accreted Carboniferous to Cretaceous submarine fan deposits [*Mortimer*, 2004] deposited on oceanic lithosphere [*Cooper and Ireland*, 2013], the ancient Re and Hf depletion ages could possibly reflect ancient remnants of depleted mantle lithosphere that have been preserved and isolated within convecting asthenosphere, brought up at a spreading center, and subsequently accreted along with overlying crust to the Gondwana margin in the Mesozoic. In fact, ancient Os isotope ratios have already been identified in exhumed oceanic lithospheric mantle on Macquarie Island, located in the center of a young (< 85 Ma) ocean basin that formed between Australia and Zealandia [*Dijkstra et al*., 2010].

7.2. Metasomatic Agent

Varying degrees of metasomatic enrichment are recorded in the examined Zealandia SCLM domains. Key indicators of metasomatism include the presence of wehrlites and olivine-rich lherzolites (Figure 2), the occurrence of apatite and hydrous minerals, elevated clinopyroxene Yb in samples with high spinel Cr# (Figure 3d), and the presence of LREE-enriched clinopyroxene. The cause of LREE enrichment has been long debated and several mechanisms are commonly suggested: hydrous fluids, silicate melts, and carbonatite melts. With the exception of the depletion-only Group 2 xenoliths, the trace element-isotope modeling suggests that the metasomatism was commonly of small volumes (< ~3 %) and that at least some could have been due to reaction with carbonatite (Figures 7a and 7d). However, the large number of clinopyroxene samples analyzed for trace elements in the course of this study (n = 79) provides an opportunity to examine broad geochemical trends in the Zealandia SCLM and provide a rigorous assessment into the cause(s) of metasomatism.

A prominent feature of the clinopyroxene trace element data set is the widespread occurrence of negative Ti anomalies (Figures 4 and 5). These are known to be signs of depletion [*Bizimis et al*., 2000]. However, when clinopyroxene Ti is plotted against Dy, averaged Dy commonly plots well above a depletion trend (Figure 10a). The clinopyroxene grains also show distinct enrichments in Eu relative to Ti (Figure 10b), with compositions plotting well above the depletion trend or the inferred field of peridotite modification by hydrous fluids. Metasomatism therefore added Eu and Dy but not Ti. A low Ti/Eu is thought to be indicative of carbonatite metasomatism [*Rudnick et al*., 1993; *Coltorti et al*., 1999].

Wittig et al. [2010] have discussed how partitioning of Th and U into clinopyroxene may aid distinguishing types of metasomatism. A $^{232}Th/^{238}U$ of 2.5 to 3.5 was suggested to be representative for depleted mantle and bulk silicate earth [*Wittig et al*., 2010]. As clinopyroxene partitions Th and U almost equally, metasomatism by a basaltic silicate melt should impart a similar Th/U ratio into the metasomatic pyroxene. Metasomatism by hydrous fluids, however, should impart a low Th/U on clinopyroxene due to the low solubility of Th relative to U in fluid. On the other hand, the variable but often high Th/U of

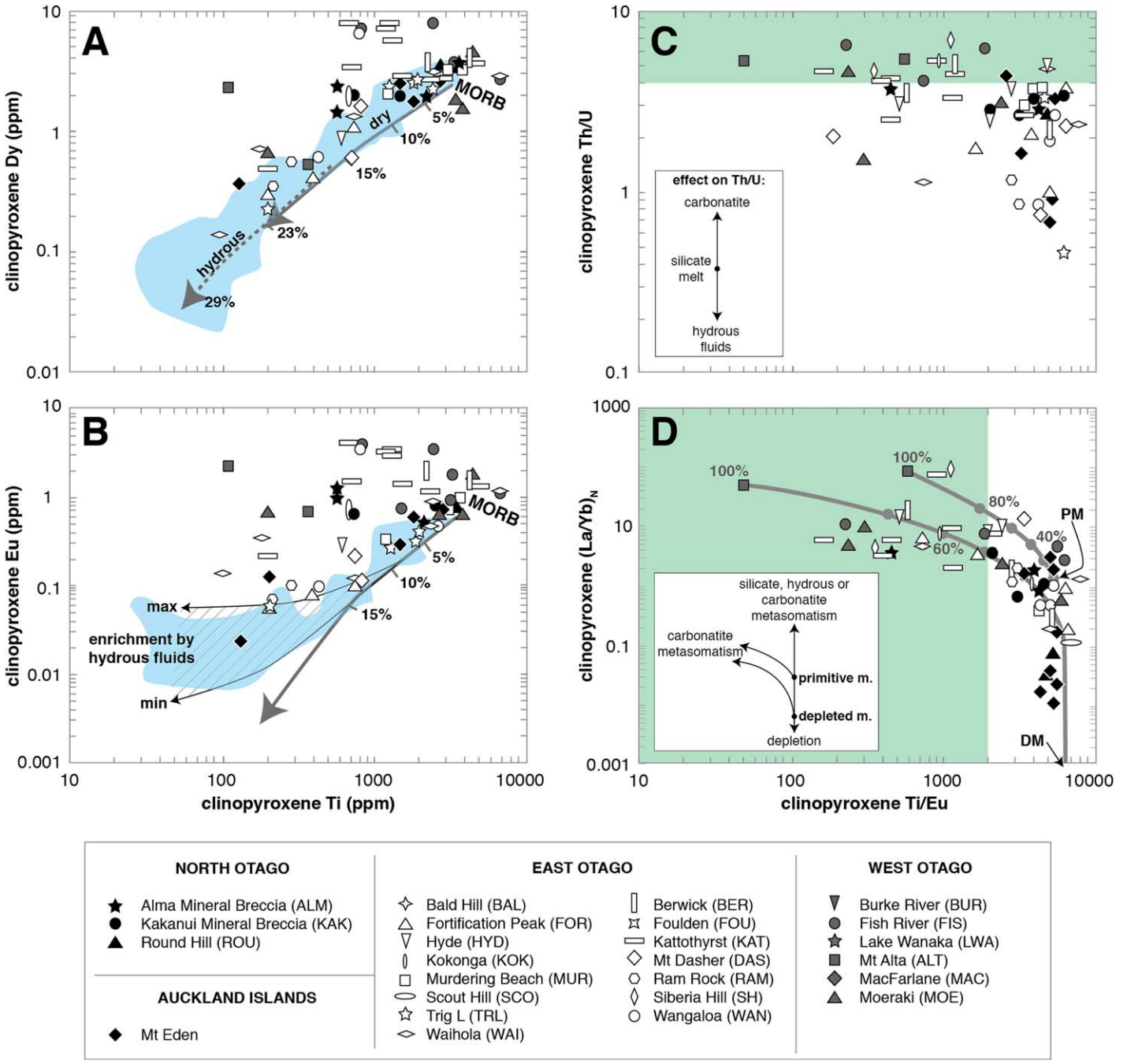

Figure 10. Clinopyroxene trace element diagrams. (a) This figure shows the expected Ti versus Dy depletion trend for clinopyroxenes in dry and wet mantle conditions. The melting trends and the blue field (a compilation of subarc mantle lithosphere clinopyroxene grains) are from *Bizimis et al.* [2000]. Zealandia data commonly fall above the depletion trend. Some data points have been omitted for clarity in the vicinity of MORB. (b) Ti versus Eu indicates that most of the Zealandia peridotites plot well above the trend for enrichment by hydrous fluids. Reference fields from *Bizimis et al.* [2000]. (c) Th/U versus Ti/Eu suggests that some samples plot away from the expected values for clinopyroxene enriched by silicate melts or hydrous fluids. *Wittig et al.* [2010] suggest a Th/U value >4 (green field) may be indicative of carbonatite metasomatism. (d) Ti/Eu versus $(La/Yb)_N$ suggests that many samples have been enriched by a metasomatic agent carrying no Ti but significant amounts of Eu and La. Mixing lines are between clinopyroxene in equilibrium with Primitive Mantle or Depleted Mantle and the strongly metasomatized West Otago samples. Points on these evolution lines represent 20% increments. The green field represents the expected values for clinopyroxene peridotites that have experienced carbonatite metasomatism [see *Rudnick et al.*, 1993; *Coltorti et al.*, 1999; *Scott et al.*, 2014].

carbonatites should cause some clinopyroxene Th/U to also be extremely high. Many of the Zealandia samples with low Ti/Eu also have distinctly elevated Th/U (Figure 10c), which suggests that metasomatism was not caused by typical silicate melts or hydrous fluids. This parameter also argues against the

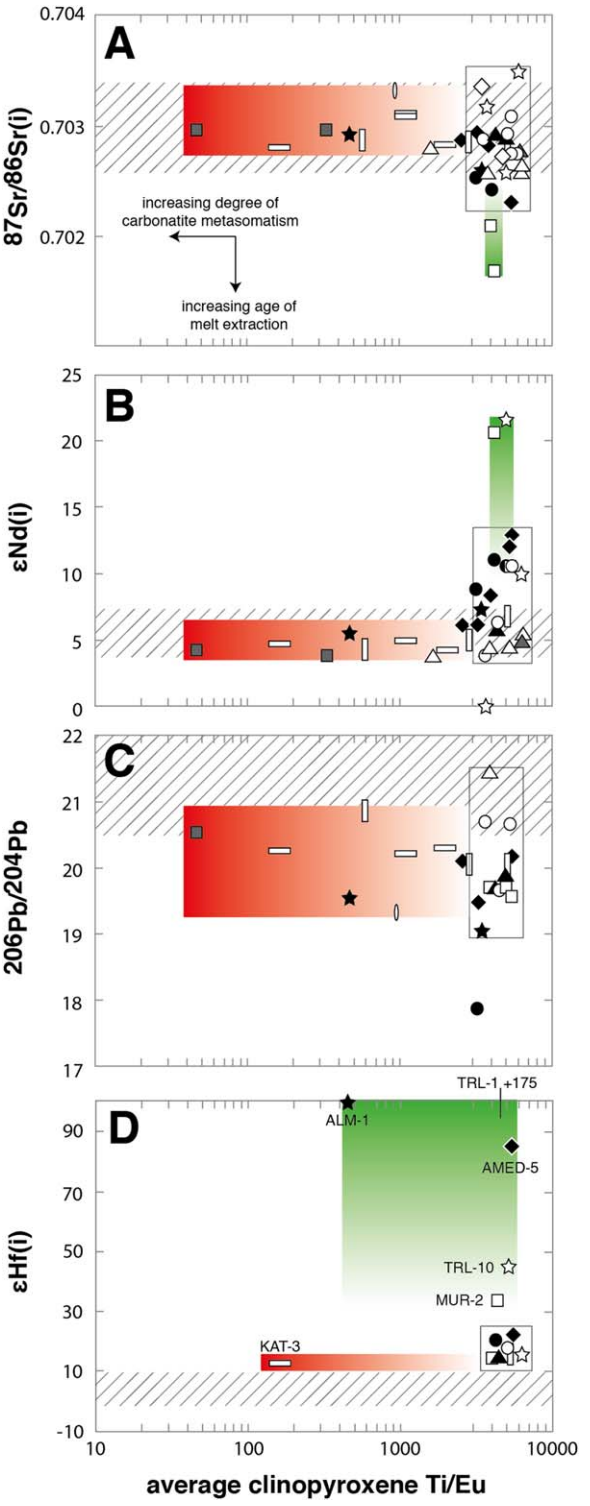

Figure 11. Average clinopyroxene Ti/Eu versus $^{87}Sr/^{86}Sr_{(i)}$ (a), $\varepsilon Nd_{(i)}$ (b), and $^{206}Pb/^{204}Pb$ (c) ratios highlight the isotopic composition of the metasomatic agent (shown in red) that has affected areas of the Zealandia SCLM. Anciently depleted samples have a green background. The HIMU isotopic field is indicated by the hatched area (data from *Stracke et al*., [2003] and *Nebel et al*., [2013]). Symbols are the same as in Figure 10. (d) Hf isotopes in several instances (ALM-1, AMED-5, MUR-2, TRL-1, and TRL-10) record ancient depletion and decoupling from metasomatism, which is expected to have a significantly less radiogenic composition (KAT-3).

metasomatism having originated from reaction with the host (silicate) basalts. Samples with low clinopyroxene Ti/Eu also have elevated normalized La/Yb (Figure 10d). The peridotites with low $(La/Yb)_N$ are those that have undergone melt depletion followed by little or no LREE enrichment, whereas those with $(La/Yb)_N \geq 1$ have undergone little or no depletion and/or experienced LREE-enrichment. It will be the formerly most depleted samples that preserve the best evidence for metasomatism because there is little, if any, preexisting clinopyroxene to dilute the metasomatic signature. Unsurprisingly, it is the samples from the refractory West Otago SCLM that have the clearest signs of enrichment (Figures 5 and 10).

A feature that calls into question a carbonatite origin to metasomatism is the apparent low Nb concentrations of the clinopyroxene grains (Figures 4 and 5) [e.g., *Bizimis et al*., 2003]. In detail, however, the peridotites with the highest clinopyroxene Nb concentrations also have the highest LREE concentrations. Nb has evidently been added by metasomatism but the low overall concentrations may indicate that the Zealandia lithosphere had undergone prior extreme Nb depletion. *Shaw et al*. [2007] make a similar argument for the Arabian lithosphere.

7.3. Isotopic Composition of the Metasomatic Agents

Regardless of the exact nature of the metasomatic

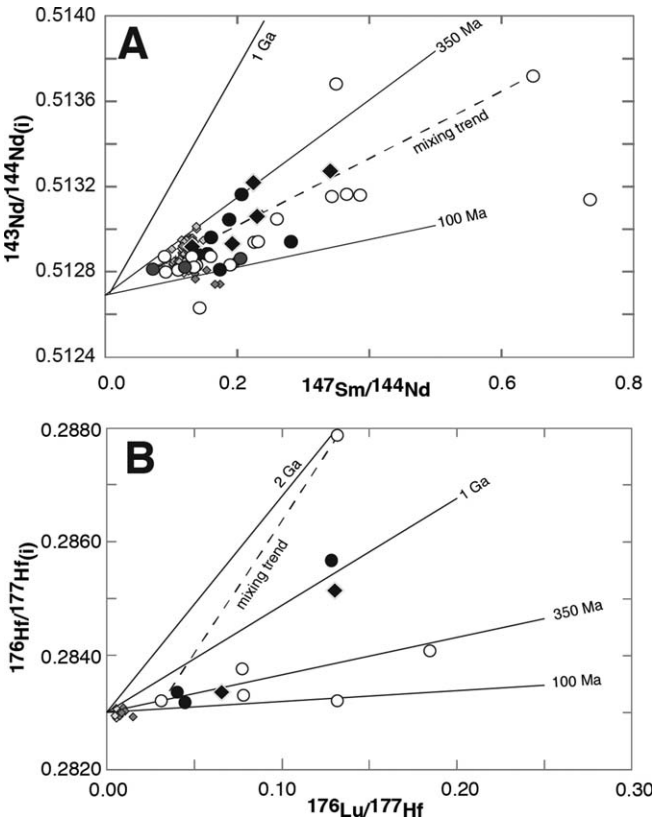

Figure 12. Clinopyroxene isochron plots. (a) $^{143}Nd/^{144}Nd$ versus $^{147}Sm/^{144}Nd$ isochron plot. (b) $^{176}Hf/^{177}Hf$ versus $^{176}Lu/^{177}Hf$ isochron plots. Hypothetical age reference lines for 100, 350, 1000, and 2000 Ma are shown, as well as a mixing trend between an enriched (MUR-1) and a depleted (TRL-1) sample (dashed line). Symbols as in Figure 6.

agent, there is no doubt that much of the SCLM beneath southern Zealandia has been enriched. Peridotites with low Ti/Eu (our preferred proxy for the clearest metasomatic signature) have restricted Sr and Nd isotopic compositions ($^{87}Sr/^{86}Sr \approx 0.703$, $\varepsilon Nd_i \approx +4$ to $+5$) (Figures 11a and 11b). These data overlap with the field for HIMU. $^{206}Pb/^{204}Pb$ in the strongly metasomatized peridotites has a large spread and averages about 20 (Figure 11c), also close to HIMU. εHf_i is not well represented in the metasomatized samples and more data are required to make a conclusive statement; however, it is notable that the εHf_i in KAT-3 plots close to HIMU field (Figure 11d). ALM-1, another metasomatized sample, has extremely radiogenic εHf of $+99$ but εNd of $+5.3$ (Figure 11b). The degree of decoupling of isotopes could be due to reaction with carbonatite because less than 1 percent metasomatic agent will swamp a depleted Nd isotope signal, whereas several percent are required to overprint the Hf isotope signature, depending on the timing of depletion (Figures 8e and 8f).

The observation that the strongly metasomatized samples have different Sm/Nd ratios yet very similar Nd isotope ratios (supporting information Table 2) suggests that the metasomatism that affected much of southern Zealandia was likely relatively recent and radiogenic ingrowth is not yet detectable. The broad positive correlation between $^{147}Sm/^{144}Nd$ and $^{143}Nd/^{144}Nd_i$, which can be encompassed by 100 and 350 Ma isochrons (Figure 12a), may place broad constraints on the timing of metasomatism. A number of the samples similarly form a broad correlation between $^{176}Lu/^{177}Hf$ and $^{176}Hf/^{177}Hf$ that falls within the 100 and 350 Ma isochrons (Figure 12b). In the Carboniferous, the paleo-Pacific Gondwana subduction margin was affected by regional tectonism and magmatism [*Tulloch et al*., 2009a, 2009b; *Scott et al*., 2011] followed by broad quiescence until the Jurassic-Early Cretaceous. However, as shown in Figures 8e and 8f, these trends could also be consistent with modern mixing between an ancient depleted component (radiogenic $^{143}Nd/^{144}Nd$ and $^{176}Hf/^{177}Hf$ and high Sm/Nd and Lu/Hf) and an enriched component. In any case, peridotites with extreme εHf fall off the 100–350 Ma trend and confirm that long periods of isolation are necessary to explain their Hf isotopic compositions.

The occurrence of a HIMU-like isotopic signature beneath the continental lithospheric peridotitic mantle has been documented from off-cratonic xenoliths in locations other than Zealandia. Peridotite xenoliths from northern Africa [*Beccaluva et al*., 2007, 2008; *Wittig et al*., 2010; *Malarkey et al*., 2011], Jordan [*Shaw et al*., 2007], Germany [*Witt-Eickschen et al*. 2003], and Antarctica [*Martin et al*., 2013] show signs of reaction with metasomatic agents with HIMU-like isotopic signatures. In each location, at least several of the peridotites have clinopyroxene grains bearing low Ti/Eu and elevated LREE that suggest enrichment by carbonatites or CO_2-rich fluids. HIMU-like isotopic signatures in the SCLM may be globally linked to CO_2-rich melts.

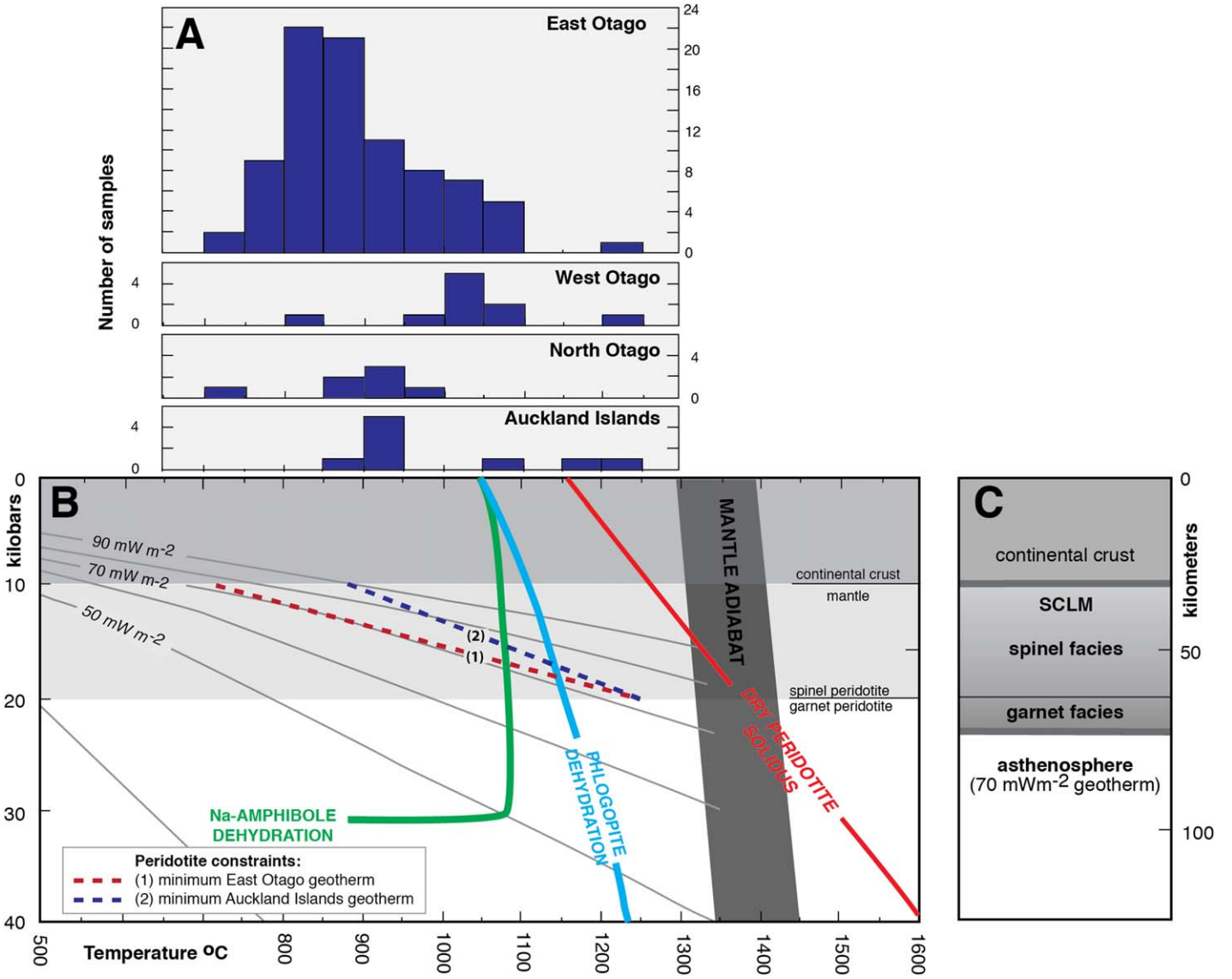

Figure 13. (a) A summary of the geothermometric estimates (calculated for 15 kbar). (b) Using the maximum and minimum temperatures for East Otago and the Auckland Islands data sets, and assuming P of 10 and 20 kbar representing the spinel facies for lherzolite, minimum geotherms can be constructed for different regions (dashed lines). The peridotite temperatures and geotherms extrapolated onto a crust mantle profile to define the approximate petrological base of the Zealandia Oligocene-Miocene lithosphere (c). These lines indicate that the geotherm beneath southern Zealandia was ~70 mWm^{-2} (or hotter) and should intercept the mantle adiabat at around 70 km depth. Present-day crustal heat flow measurements for the South Island of New Zealand vary between ~60 and 90 mWm^{-2} [*Godfrey et al*., 2001], with the lowest measurements coming from areas composed of uplifted sedimentary basins in which a higher heat-flow could have been suppressed by shallow circulating water. Neither amphibole nor phlogopite is stable at the temperatures near the base of the Zealandia lithosphere. Dehydration curves are from *Frost* [2006]; dry peridotite solidus is from *Katz et al*. [2003]; amphibole dehydration is from *Green et al*. [2010]; geotherms are from *Furlong and Chapman* [2013].

7.4. A SCLM Source to the Zealandia Intraplate Basalts?

The goal established at the beginning of this study was to determine whether the Zealandia SCLM could have contributed to the widespread intraplate basalts with HIMU-like signatures. The peridotite data presented above show that the Zealandia SCLM does, in places, have a HIMU-like imprint. The data also reveal that the previously assumed Zealandia SCLM isotopic composition of $^{87}Sr/^{86}Sr > 0.7035$, $^{143}Nd/^{144}Nd < 0.5128$, and $^{206}Pb/^{204}Pb = 18.7–18.9$ is incorrect. The Zealandia intraplate basalts have been subdivided into low-silica (~43–48 wt %) and high-silica (48–55 wt %) variants, with the low silica variants having stronger HIMU-like isotopic source signatures [*Hoernle et al*., 2006; *Sprung et al*., 2007]. There are distinct isotopic similarities between the low-silica basalts and a number of the peridotite xenoliths (Figures 6a–6d). However, Figure 6e reveals that the peridotites are mostly more radiogenic in Nd

and Hf than the intraplate basalts. Furthermore, a problem with comparing spinel peridotites with the intraplate basalts is that the latter group displays various trace element parameters that suggest the presence of residual garnet peridotite [*Panter et al*., 2006; *Sprung et al*., 2007; *Timm et al*., 2009; *Scott et al*., 2013] with or without eclogite or garnet pyroxenite [*Hoernle et al*., 2006; *McCoy-West et al*., 2010; *Timm et al*., 2010; *McGee et al*., 2013]. The hot temperatures calculated for the spinel facies peridotites, reaching up to 1100–1260°C (Figure 13a), mean that the geotherm beneath Zealandia must be hot ($\sim$70 mWm^2) and would likely intercept the adiabat at $<$ 80 km depth (Figures 13b and 13c). The Zealandia garnet facies peridotitic SCLM, if even present, must therefore be very thin. If the studied spinel peridotite samples are representative of the shallow SCLM, then the thin garnet facies lithosphere can only be the source of the low-silica basalts if (1) the melted components had a different time-integrated history of trace element depletion and enrichment that resulted in less radiogenic Nd and Hf; and/or (2) the chemistry of the basalts formed by a process other than pure melting of lithosphere in the presence of residual garnet. Possible scenarios involve mixing of SCLM with less radiogenic Hf-bearing melts emanating from the asthenosphere, or melting and mixing of a lithologically heterogeneous lithosphere containing garnet-bearing enriched domains of eclogite or pyroxenite. In the absence of garnet peridotite and other enriched xenoliths, these hypotheses remain to be tested.

The peridotite isotope data do offer insights into the formation of the high silica basalts, which have isotopic compositions that have been attributed to lithosphere contamination [e.g., *Hoernle et al*., 2006]. Although the high-silica basalts overlap with the peridotites in terms of Sr, Nd, and Pb (Figures 6a–6d), there is very little overlap in Hf-Nd isotope space (Figure 6e). The high-silica intraplate basalts show a trend toward less radiogenic ^{206}Pb/^{204}Pb and ^{143}Nd/^{144}Nd and more radiogenic ^{87}Sr/^{86}Sr and ^{207}Pb/^{204}Pb ratios than occur in the peridotite suite (Figure 6a–6c). On this basis, contamination by shallow lithospheric mantle cannot explain the observed isotopic trends in the high-silica basalts. An alternative explanation is that these basalts represent contamination of low-silica basalt by continental crust [e.g., *Tappenden*, 2003; *Panter et al*., 2006; *McCoy-West et al*., 2010]. Metasedimentary rocks dominate the upper crust of the central South Island and host many of the intraplate basalts. Equivalents to these metasediments in the North Island have isotopic compositions of ^{143}Nd/^{144}Nd = 0.5124, ^{176}Hf/^{177}Hf = 0.2826, ^{87}Sr/^{86}Sr = 0.708–0.712, ^{206}Pb/^{204}Pb = 18.8–18.9, ^{207}Pb/^{204}Pb = 15.6 [*Price et al*., 2012] (Waight, unpublished data, 2014) that would, if mixed with low-silica basalt, shift the basalt isotopic compositions away from the HIMU field.

8. Conclusions

We have presented the first description of the regional composition of the Oligocene-Miocene subcontinental lithospheric mantle beneath Zealandia. This thin SCLM had a highly refractory craton-like domain (West Otago) situated adjacent to the moderately fertile (East Otago, North Otago, and Auckland Islands) domains. In some cases, this SCLM experienced depletion at $\sim$ 2 Ga. There is no obvious translithospheric suture that separates domains, but this may be because inspected portions of the Zealandia SCLM have early histories decoupled from the overlying continental crust. The ancient SCLM beneath Zealandia may have remained stable for billions of years [*McCoy-West et al*., 2013] or it may represent ancient lithosphere that has passed through the asthenosphere, upwelled, and then accreted to Gondwana during Mesozoic subduction.

Mantle metasomatism has affected many portions of the Zealandia SCLM. Trace elements in clinopyroxene strongly suggest that the metasomatic agent was carbonatitic. The intensity of the metasomatism is variable, but clinopyroxene isotopes from the most affected peridotites indicate that the metasomatizing agent had an approximate HIMU-like isotopic character of ^{87}Sr/^{86}Sr $\approx$ 0.703, εNd $\approx +5$, and ^{206}Pb/^{204}Pb $\approx$ 20. Although the Zealandia intraplate basalts also have a HIMU-like signature, trace elements suggest they have garnet peridotite in their source region and therefore cannot be derived from SCLM represented by the studied spinel facies xenoliths investigated here. Assuming that the studied spinel facies xenoliths are broadly representative of the thin Zealandia SCLM, clinopyroxene Hf isotope data indicate that the less radiogenic basalts could only be derived from garnet facies SCLM if this thin lower lithosphere either (1) has a less radiogenic Hf composition than the spinel facies, or (2) was mixed with melts originating from a less radiogenic Hf asthenospheric source.

Acknowledgments
The project was funded by a New Zealand Foundation for Research Science and Technology Post-Doctoral Fellowship contract UOX1004 to JMS and a Danish Research Council for Nature and Universe grant to TEW. The New Zealand Department of Conservation permitted collection of xenoliths. We greatly thank M. Bizimis, M. Jackson, N. Wittig and an anonymous reviewer for detailed comments that helped to strengthen and clarify our study.

References

Baker J. A., J. A. Gamble, and I. J. Graham (1994), The age, geology and geochemistry of the Tapuaenuku Igneous Complex, Marlborough, New Zealand, *N. Z. J. Geol. Geophys.*, *37*, 249–268.

Bernstein, S., P. B. Kelemen, and K. Hanghøj (2007), Consistent olivine Mg# in cratonic mantle reflects Archean mantle melting to the exhaustion of orthopyroxene, *Geology*, *35*(5), 459–462.

Barreiro B. A., and A. F. Cooper (1987), A Sr, Nd, and Pb isotope study of alkaline lamprophyres and related rocks from Westland and Otago, South Island, New Zealand, *Spec. Pap. Geol. Soc. Am.*, *215*, 115–125.

Beccaluva, L., A. Azzouni-Sekkal, A. Benhallou, G. Bianchini, R. M. Ellam, M. Marzola, F. Sienna, and F. M. Stuart (2007), Intracratonic asthenosphere upwelling and lithosphere rejuvenation beneath the Hoggar swell (Algeria): Evidence from HIMU metasomatized lherzolite mantle xenoliths. *Earth Planet. Sci. Lett.*, *260*(3), 482–494.

Beccaluva, L., G. Bianchini, R. M. Ellam, M. Marzola, K. M. Oun, F. Siena, and F. M. Stuart (2008), The role of HIMU metasomatic components in the North African lithospheric mantle: Petrological evidence from the Gharyan lherzolite xenoliths, NW Libya, *Geol. Soc. Spec. Publ.*, *293*(1), 253–277.

Bizimis, M., V. J. Salters, and E. Bonatti (2000), Trace and REE content of clinopyroxenes from supra-subduction zone peridotites: Implications for melting and enrichment processes in island arcs, *Chem. Geol.*, *165*(1), 67–85.

Bizimis, M., V. J. Salters, and J. B. Dawson (2003a), The brevity of carbonatite sources in the mantle: Evidence from Hf isotopes. *Contrib. Mineral. Petrol.*, *145*(3), 281–300.

Bizimis, M., G. Sen, and V. J. M. Salters (2003b), Hf-Nd isotope decoupling in the oceanic lithosphere: Constraints from spinel peridotites from Oahu, Hawaii, *Earth Planet. Sci. Lett.*, *217*, 43–58.

Bizimis, M., M. Griselin, J. C. Lassiter, V. J. Salters, and G. Sen (2007), Ancient recycled mantle lithosphere in the Hawaiian plume: Osmium–Hafnium isotopic evidence from peridotite mantle xenoliths, *Earth Planet. Sci. Lett.*, *257*(1), 259–273.

Boyd, F. R. (1989), Compositional distinction between oceanic and cratonic lithosphere, *Earth Planet. Sci. Lett.*, *96*(1), 15–26.

Bradshaw, J. D. (1989), Cretaceous geotectonic patterns in the New Zealand region, *Tectonics*, *8*(4), 803–820.

Brandon, A. D., J. E. Snow, R. J. Walker, J. W. Morgan, and T. D. Mock (2000), ^{190}Pt–^{186}Os and ^{187}Re–^{187}Os systematics of abyssal peridotites, *Earth Planet. Sci. Lett.*, *177*, 319–335.

Brodie C. G., and Cooper A. F. (1989), Nodule associations from ouachitite and camptonite lamprophyres, western Otago and south Westland, New Zealand, *Geol. Soc. Aust. Spec. Publ.*, *14* 545–559.

Brown D. A. (1954), The geology of Siberia Hill and Mount Dasher, North Otago, *Trans. R. Soc. New Zealand 83*, 347–372.

Carlson, R. W., D. G. Pearson, and D. E. James (2005), Physical, chemical, and chronological characteristics of continental mantle, *Rev. Geophys.*, *43*, RG1001, doi:10.1029/2004RG000156.

Carswell, D. A. (1980), Mantle derived lherzolite nodules associated with kimberlite, carbonatite and basalt magmatism: A review. *Lithos*, *13*(2), 121–138.

Chase, C. G. (1981), Oceanic island Pb: 2-stage histories and mantle evolution, *Earth Planet. Sci. Lett.*, *52*, 277–284.

Coltorti, M., C. Bonadiman, R. W. Hinton, F. Siena, and B. G. J. Upton (1999), Carbonatite metasomatism of the oceanic upper mantle: Evidence from clinopyroxenes and glasses in ultramafic xenoliths of Grande Comore, Indian Ocean, *J. Petrol.*, *40*(1), 133–165.

Cook, C., R. M. Briggs, I. E. Smith, and R. Maas (2005), Petrology and geochemistry of intraplate basalts in the South Auckland volcanic field, New Zealand: Evidence for two coeval magma suites from distinct sources, *J. Petrol.*, *46*(3), 473–503.

Coombs, D. S., R. A. Cas, Y. Kawachi, C. A. Landis, W. F. McDonough, and A. Reay (1986), Cenozoic volcanism in North, East, and Central Otago, in I. E. M. Smith, Late Cenozoic volcanism in New Zealand, *Bull. R. Soc. N. Z.*, *23*,278–312.

Coombs D. S., C. J. Adams, B. P. Roser, and A. Reay (2008), Geochronology and geochemistry of the Dunedin Volcanic Group, eastern Otago, New Zealand, *N. Z. J. Geol. Geophys.*, *51*, 195–218.

Cooper, A. F. (1986), A carbonatitic lamprophyre dike swarm from the Southern Alps, Otago and Westland, in I. E. M. Smith, Late Cenozoic volcanism in New Zealand, *Bull. R. Soc. N. Z.*, *23*, 313–336.

Cooper, A. F., and T. R. Ireland (2013), Cretaceous sedimentation and metamorphism of the western Alpine Schist protoliths associated with the Pounamu Ultramafic Belt, Westland, New Zealand, *N. Z. J. Geol. Geophys.*, *56*(4), 188–199.

Cooper, A. F., and L. A. Paterson (2008), Carbonatites from a lamprophyre dyke swarm, south Westland, New Zealand, *Can. Mineral.*, *46*(4), 753–777.

Cooper, A. F., B. A. Barreiro, D. L. Kimbrough, and J. M. Mattinson (1987), Lamprophyre dike intrusion and the age of the Alpine fault, New Zealand, *Geology*, *15*, 941–944.

Dautria, J. M., C. Dupuy, D. Takherist, and J. Dostal (1992), Carbonate metasomatism in the lithospheric mantle: Peridotitic xenoliths from a melilititic district of the Sahara basin, *Contrib. Mineral. Petrol.*, *111*(1), 37–52.

Dick, H. J., and T. Bullen (1984), Chromian spinel as a petrogenetic indicator in abyssal and alpine-type peridotites and spatially associated lavas, *Contrib. Mineral. Petrol.*, *86*(1), 54–76.

Dijkstra, A. H., D. S. Sergeev, C. Spandler, T. Pettke, T. Meisel, and P. A. Cawood (2010), Highly refractory peridotites on Macquarie Island and the case for anciently depleted domains in the Earth's mantle, *J. Petrol.*, *51*(1-2), 469–493.

Douglas, B. J. (1986), Lignite resources of central Otago, *Publ. PI04*, N. Z. Energ. Res. and Dev. Comm, 368 pp.

Downes, H. (2001), Formation and modification of the shallow sub-continental lithospheric mantle: A review of geochemical evidence from ultramafic xenolith suites and tectonically emplaced ultramafic massifs of western and central Europe, *J. Petrol.*, *42*(1), 233–250.

Duclos M., M. K. Savage, A. Tommasi, and K. R. Gledhill (2005), Mantle tectonics beneath New Zealand inferred from SKS splitting and petrophysics, *Geophys. J. Int.*, *163*, 760–774.

Eggins, S. M., R. L. Rudnick, and W. F. McDonough (1998), The composition of peridotites and their minerals: A laser-ablation ICP-MS study, *Earth Planet. Sci. Lett.*, *154*, 53–71.

Finn, C. A., R. D. Müller, and K. S. Panter (2005), A Cenozoic diffuse alkaline magmatic province (DAMP) in the southwest Pacific without rift or plume origin, *Geochem. Geophys. Geosyst.*, *6*, Q02005, doi:10.1029/2004GC000723.

Forsyth, P. J., G. M. Martin, H. J. Campbell, and J. E., Simes (2006), Carboniferous conodonts from the Rakaia Terrane, East Otago, New Zealand, *N. Z. J. Geol. Geophys.*, *49*, 329–336.

Frost, D. J. (2006), The stability of hydrous mantle phases, *Rev. Mineral. Geochem.*, *62*(1), 243–271.

Furlong, K. P., and D. S. Chapman (2013), Heat flow, heat generation, and the thermal state of the lithosphere, *Annu. Rev. Earth Planet. Sci.*, *41*, 385–410.

Gaina, C., D. R. Müller, J. Y. Royer, J. Stock, J. Hardebeck, and P. Symonds (1998), The tectonic history of the Tasman Sea: A puzzle with 13 pieces, *J. Geophys. Res.*, *103*(B6), 12,413–12,433.

Gamble J. A., P. A. Morris, and C. J. Adams (1986), The geology, petrology and geochemistry of Cenozoic volcanic rocks from the Campbell Plateau and Chatham Rise, *Bull. R. Soc. N. Z.*, *23*, 344–365.
Gibson, G. M., I. McDougall, and T. R. Ireland (1988), Age constraints on metamorphism and the development of a metamorphic core complex in Fiordland, southern New Zealand, *Geology*, *16*(5), 405–408.
Godfrey, N. J., F. Davey, T. A. Stern, and D. Okaya (2001), Crustal structure and thermal anomalies of the Dunedin region, South Island, New Zealand, *J. Geophys. Res.*, *106*(B12), 30,835–30,848.
Green, D. H., W. O. Hibberson, I. Kovács, and A. Rosenthal (2010), Water and its influence on the lithosphere-asthenosphere boundary, *Nature*, *467*(7314), 448–451.
Griffin, W. L., A. F. Kobussen, E. V. S. S. K. Babu, S. Y. O'Reilly, R. Norris, and P. Sengupta (2009a), A translithospheric suture in the vanished 1-Ga lithospheric root of South India: Evidence from contrasting lithosphere sections in the Dharwar Craton, *Lithos*, *112*, 1109–1119.
Griffin, W. L., S. Y. O'Reilly, J. C. Afonso, and G. C. Begg (2009b), The composition and evolution of lithospheric mantle: A re-evaluation and its tectonic implications, *J. Petrol.*, *50*(7), 1185–1204.
Griffin, W. L., N. Nikolic, S. Y. O'Reilly, and N. J. Pearson (2012), Coupling, decoupling and metasomatism: Evolution of crust–mantle relationships beneath NW Spitsbergen, *Lithos*, *149*, 115–135.
Hart, S. R. (1984), A large scale isotope anomaly in the Southern Hemisphere mantle, *Nature 309*, 753–757.
Hart, S. R., J. Blusztajn, W. E. LeMasurier, and D. C. Rex (1997), Hobbs Coast Cenozoic volcanism: Implications for the West Antarctic rift system. *Chem. Geol.*, *139*(1), 223–248.
Harte, B. (1977), Rock nomenclature with particular relation to deformation and recrystallization textures in olivine-bearing xenoliths, *J. Geol.*, *85*, 279–288.
Harvey, J., A. Gannoun, K. W. Burton, N. W. Rogers, O. Alard, and I. J. Parkinson (2006), Ancient melt extraction from the oceanic upper mantle revealed by Re–Os isotopes in abyssal peridotites from the Mid-Atlantic ridge, *Earth Planet. Sci. Lett.*, *244*, 606–621.
Hellebrand, E., J. E. Snow, H. J. Dick, and A. W. Hofmann (2001), Coupled major and trace elements as indicators of the extent of melting in mid-ocean-ridge peridotites, *Nature*, *410*(6829), 677–681.
Hoernle, K., J. D. L. White, P. van den Bogaard, F. Hauff, D. S. Coombs, R. Werner, C. Timm, D. Garbe-Schönberg, A. Reay, and A. F. Cooper (2006), Cenozoic intraplate volcanism on New Zealand: Upwelling induced by lithospheric removal, *Earth Planet. Sci. Lett.*, *248*, 350–367.
Hofmann, A. W. (2003), Sampling mantle heterogeneity through oceanic basalts: Isotopes and trace elements, *Treat. Geochem.*, *2*, 61–101.
Hofmann, A. W., and W. M. White (1982), Mantle plumes from ancient oceanic crust, *Earth Planet. Sci. Lett.*, *57*, 421–436.
Hoke, L., R. Poreda, A. Reay, and S. D. Weaver (2000), The subcontinental mantle beneath southern New Zealand, characterized by helium isotopes in intraplate basalts and gas-rich springs, *Geochim. Cosmochim. Acta*, *64*, 2489–2507.
Ionov, D. A., C. Dupuy, S. Y. O'Reilly, M. G. Kopylova, and Y. S. Genshaft (1993), Carbonated peridotite xenoliths from Spitsbergen: Implications for trace element signature of mantle carbonate metasomatism, *Earth Planet. Sci. Lett.*, *119*(3), 283–297.
Katz, R. F., M. Spiegelman, and C. H. Langmuir (2003), A new parameterization of hydrous mantle melting, *Geochem. Geophys. Geosyst.*, *4*(9), 1073, doi:10.1029/2002GC000433.
Kipf, A., F. Hauff, R. Werner, K. Gohl, P. van den Bogaard, K. Hoernle, D. Maicher, and A. Klügel (2013), Seamounts off the West Antarctic margin: A case for non-hotspot driven intraplate volcanism, *Gondwana Res.*, *25*, 1660–1679.
Klemme, S. (2004), The influence of Cr on the garnet–spinel transition in the Earth's mantle: Experiments in the system $MgO–Cr_2O_3–SiO_2$ and thermodynamic modeling, *Lithos*, *77*(1), 639–646.
Landis, C. A., and D. S. Coombs (1967), Metamorphic belts and orogenesis in southern New Zealand, *Tectonophysics*, *4*(4), 501–518.
Lanyon, R., R. Varne, and A. J. Crawford (1993), Tasmanian Tertiary basalts, the Balleny plume, and opening of the Tasman Sea (southwest Pacific Ocean), *Geology*, *21*(6), 555–558.
Lee, C. T., Q. Yin, R. L. Rudnick, and S. B. Jacobsen (2001), Preservation of ancient and fertile lithospheric mantle beneath the southwestern United States, *Nature*, *411*(6833), 69–73.
Lee, C. T. A., P. Luffi, and E. J. Chin (2011), Building and destroying continental mantle, *Annu. Rev. Earth Planet. Sci.*, *39*, 59–90.
Liu, C. Z., J. E. Snow, E. Hellebrand, G. Brügmann, A. von der Handt, A. Büchl, and A. W. Hofmann (2008), Ancient, highly heterogeneous mantle beneath Gakkel ridge, Arctic Ocean, *Nature*, *452*(7185), 311–316.
Liu, J., R. W. Carlson, R. L. Rudnick, R. J. Walker, S. Gao, and F.-Y. Wu (2012), Comparative Sr-Nd-Hf-Os-Pb isotope systematics of xenolithic peridotites from Yangyuan, North China Craton: Additional evidence for a Paleoproterozoic age, *Chem. Geol.*, *332–333*, 1–14.
Liu, J., R. L. Rudnick, R. J. Walker, W. L. Xu, S. Gao, and F. Y. Wu (2014), Big insights from tiny peridotites: Evidence for persistence of Precambrian lithosphere beneath the eastern North China Craton, *Tectonophysics*, in press.
McCoy-West, A. J., J. A. Baker, K. Faure, and R. Wysoczanski (2010), Petrogenesis and origins of mid-Cretaceous continental intraplate volcanism in Marlborough, New Zealand: Implications for the long-lived HIMU magmatic mega-province of the SW Pacific, *J. Petrol.*, *51*(10), 2003–2045.
McCoy-West, A. J., V. C. Bennett, I. S. Puchtel, and R. J. Walker (2013), Extreme persistence of cratonic lithosphere in the southwest Pacific: Paleoproterozoic Os isotopic signatures in Zealandia, *Geology*, *41*(2), 231–234.
McGee, L. E., I. E. Smith, M. A. Millet, H. K. Handley, and J. M. Lindsay (2013), Asthenospheric control of melting processes in a monogenetic basaltic system: A case study of the Auckland Volcanic Field, New Zealand, *J. Petrol.*, *54*(10), 2125–2153.
Malarkey, J., N. Wittig, D. G. Pearson, and J. P. Davidson (2011), Characterising modal metasomatic processes in young continental lithospheric mantle: A microsampling isotopic and trace element study on xenoliths from the Middle Atlas Mountains, Morocco, *Contrib. Mineral. Petrol.*, *162*(2), 289–302.
Martin, A. P., A. F. Cooper, and R. C. Price (2013), Petrogenesis of Cenozoic, alkalic volcanic lineages at Mount Morning, West Antarctica and their entrained lithospheric mantle xenoliths: Lithospheric versus asthenospheric mantle sources, *Geochim. Cosmochim. Acta*, *122*, 127–152.
McDonough, W. F. (1990), Constraints on the composition of the continental lithospheric mantle, *Earth Planet. Sci. Lett.*, *101*(1), 1–18.
Mortimer, N. (2004), New Zealand's geological foundations, *Gondwana Res.*, *7*(1), 261–272.
Mortimer, N., P. B. Gans, F. Hauff, and D. H. N. Barker (2012), Paleocene MORB and OIB from the Resolution Ridge, Tasman Sea, *Aust. J. Earth Sci.*, *59*(6), 953–964.
Münker, C., and R. Cooper (1999), The Cambrian arc complex of the Takaka Terrane, New Zealand: An integrated stratigraphical, paleontological, and geochemical approach, *N. Z. J. Geol. Geophys.*, *42*(3), 415–445.
Nasir, S. J., J. L. Everard, M. P. McClenaghan, D. Bombardieri, and M. A. Worthing (2010), The petrology of high pressure xenoliths and associated Cenozoic basalts from Northeastern Tasmania, *Lithos*, *118*(1), 35–49.
Nebel, O., R. J. Arculus, W. van Westrenen, J. D. Woodhead, F. E. Jenner, Y. J. Nebel-Jacobsen, M. Wille, and S. M. Eggins (2013), Coupled Hf–Nd–Pb isotope co-variations of HIMU oceanic island basalts from Mangaia, Cook-Austral islands, suggest an Archean source component in the mantle transition zone, *Geochim. Cosmochim. Acta*, *112*, 87–101.

Niu, N., C. H. Langmuir, and R. J. Kinzler (1997), The origin of abyssal peridotites: A new perspective, *Earth Planet. Sci. Lett.*, *152*, 251–265.
O'Reilly, S. Y., and W. L. Griffin (2000), Apatite in the mantle: Implications for metasomatic processes and high heat production in Phanerozoic mantle, *Lithos*, *53*(3), 217–232.
Panter, K. S., S. R. Hart, P. Kyle, J. Blusztanjn, and T. Wilch (2000), Geochemistry of Late Cenozoic basalts from the Crary Mountains: Characterization of mantle sources in Marie Byrd Land, Antarctica, *Chem. Geol.*, *165*(3), 215–241.
Panter, K. S., J. Blusztajn, S. R. Hart, P. R. Kyle, R. Esser, and W. C. McIntosh (2006), The origin of HIMU in the SW Pacific: Evidence from intraplate volcanism in southern New Zealand and the Subantarctic Islands, *J. Petrol. 47*, 1673–1704.
Parkinson, I. J., C. J. Hawkesworth, and A. S. Cohen (1998), Ancient mantle in a modern arc: Osmium isotopes in Izu-Bonin-Mariana forearc peridotites, *Science*, *281*(5385), 2011–2013.
Pearson D.G., and N. Wittig (2014), The formation and evolution of cratonic mantle lithosphere: Evidence from mantle xenoliths, in *Treatise on Geochemistry*, 2nd ed., edited by H. D. Holland and K. K. Turekian, pp. 255–292, Elsevier, Oxford.
Pearson, D. G., D. Canil, and S. B. Shirey (2003), Mantle samples included in volcanic rocks: Xenoliths and diamonds, *Treat. Geochem.*, *2*, 171–275.
Price, R. C., and R. C. Wallace (1976), The significance of corona textured inclusions from a high pressure fractionated alkalic lava: North Otago, New Zealand, *Lithos*, *9*(4), 319–329.
Price, R. C., A. F. Cooper, J. D. Woodhead, and I. A. N. Cartwright (2003), Phonolitic Diatremes within the Dunedin Volcano, South Island, New Zealand, *J. Petrol.*, *44*(11), 2053–2080.
Price, R. C., J. A. Gamble, I. E. M. Smith, R. Maas, T. E. Waight, R. B. Stewart, and J. Woodhead (2012), The anatomy of an andesitic volcano: A time-stratigraphic study of andesite petrogenesis and crustal evolution at Ruapehu Volcano, New Zealand, *J. Petrol.*, *53*, 2139–2189.
Rattenbury, M. S., R. Jongens, and S. C. Cox (2010), *Geology of the Haast Area, Institute of Geological and Nuclear Sciences 1:250000 Geological Map 14*.
Rampone, E., and A. Hofmann (2012), A global overview of isotopic heterogeneities in the oceanic mantle, *Lithos*, *148*, 247–261.
Reay, A., and P. P. Sipiera (1987), Mantle xenoliths from the New Zealand region, in *Mantle Xenoliths*, pp. 347–358, John Wiley, Chichester, U. K.
Robinson, J. A. C., and B. J. Wood (1998), The depth of the spinel to garnet transition at the peridotite solidus, *Earth Planet. Sci. Lett.*, *164*(1), 277–284.
Rocchi, S., P. Armienti, M. D'Orazio, S. Tonarini, J. R. Wijbrans, and G. Di Vincenzo (2002), Cenozoic magmatism in the western Ross Embayment: Role of mantle plume versus plate dynamics in the development of the West Antarctic Rift System, *J. Geophys. Res.*, *107*(B9), ECV-5-1–ECV-5–22.
Rocholl, A., M. Stein, M. Molzahn, S. R. Hart, and G. Wörner (1995), Geochemical evolution of rift magmas by progressive tapping of a stratified mantle source beneath the Ross Sea Rift, Northern Victoria Land, Antarctica, *Earth Planet. Sci. Lett.*, *131*(3), 207–224.
Rudnick, R. L., W. F. McDonough, and B. W. Chappell (1993), Carbonatite metasomatism in the northern Tanzanian mantle: Petrographic and geochemical characteristics, *Earth Planet. Sci. Lett.*, *114*(4), 463–475.
Salters, V. J., and A. Stracke (2004), Composition of the depleted mantle, *Geochem., Geophys. Geosyst.*, *5*, Q05B07, doi:10.1029/2003GC000597.
Salters, V. J. M., and A. Zindler (1995), Extreme $^{176}Hf/^{177}Hf$ in the sub-oceanic mantle, *Earth Planet. Sci. Lett.*, *129*, 13–30.
Sewell, R. J., B. J. Hobden, and S. D. Weaver (1993), Mafic and ultramafic mantle and deep crustal xenoliths from Banks Peninsula, South Islands, New Zealand, *N. Z. J. Geol. Geophys.*, *36*, 233–231.
Scott, J. M., and A. F. Cooper (2006), Early Cretaceous extensional exhumation of the lower crust of a magmatic arc: Evidence from the Mount Irene Shear Zone, Fiordland, New Zealand, *Tectonics*, *25*, TC3018, doi:10.1029/2005TC001890.
Scott, J., J. Muhling, I. Fletcher, M. Billia, J. M. Palin, T. Elliot, and C. Günter (2011), The relationship of Palaeozoic metamorphism and S-type magmatism on the paleo-Pacific Gondwana margin, *Lithos*, *127*(3), 522–534.
Scott, J. M., I. M. Turnbull, A. Auer, and J. M. Palin (2013), The sub-Antarctic Antipodes Volcano: A $<$ 0.5 Ma HIMU-like Surtseyan volcanic outpost on the edge of the Campbell Plateau, New Zealand, *N. Z. J. Geol. Geophys.*, *56*(3), 134–153.
Scott J. M., A. Hodgkinson, J. M. Palin, T. E. Waight, Q. H. A. Van der Meer, and A. F. Cooper (2014), Ancient melt depletion overprinted by young metasomatism; Evolution of the New Zealand lithospheric mantle, *Contrib. Mineral. Petrol.*, *167*, 1–17.
Shaw, J. E., J. A. Baker, A. J. R. Kent, K. M. Ibrahim, and M. A. Menzies (2007), The geochemistry of the Arabian lithospheric mantle: A source for intraplate volcanism?, *J. Petrol.*, *48*(8), 1495–1512.
Simon, N. S., E. R. Neumann, C. Bonadiman, M. Coltorti, G. Delpech, M. Grégoire, and E. Widom (2008), Ultra-refractory domains in the oceanic mantle lithosphere sampled as mantle xenoliths at ocean islands, *J. Petrol.*, *49*(6), 1223–1251.
Smith, D. (1977), The origin and interpretation of spinel-pyroxene clusters in peridotite, *J. Geol.*, *85*, 476–482.
Špaček, P., L. Ackerman, G. Habler, R. Abart, and J. Ulrych (2013), Garnet breakdown, Symplectite formation and melting in Basanite-hosted peridotite xenoliths from Zinst (Bavaria, Bohemian Massif), *J. Petrol.*, *54*,1691–1723.
Sprung, P., S. Schuth, C. Münker, and L. Hoke (2007), Intraplate volcanism in New Zealand: The role of fossil plume material and variable lithospheric properties, *Contrib. Mineral. Petrol.*, *153*, 669–687.
Stracke, A., M. Bizimis, and V. J. Salters (2003), Recycling oceanic crust: Quantitative constraints, *Geochem. Geophys. Geosyst.*, *4*(3), 8003, doi:10.1029/2001GC000223.
Stracke, A., A. W. Hofmann, and S. R. Hart (2005), FOZO, HIMU, and the rest of the mantle zoo, *Geochem. Geophys. Geosyst.*, *6*, Q05007, doi:10.1029/2004GC000824.
Stracke, A., J. E. Snow, E. Hellebrand, A. von der Handt, B. Bourdon, K. Birbaum, and D. Günther (2011), Abyssal peridotite Hf isotopes identify extreme mantle depletion, *Earth Planet. Sci. Lett.*, *308*, 359–368.
Streckeisen, A. (1976), To each plutonic rock its proper name, *Earth-Science Reviews*, *12*(1), 1–33.
Sun, S. S., and W. McDonough (1989), Chemical and isotopic systematics of oceanic basalts: Implications for mantle composition and processes, *Geol. Soc. Spec. Publ.*, *42*(1), 313–345.
Tappenden, V. E. (2003), Magmatic response to the evolving New Zealand margin of Gondwana during the Mid-Late Cretaceous, PhD thesis, Univ. of Canterbury, Christchurch, New Zealand.
Taylor, W. R. (1998), An experimental test of some geothermometer and geobarometer formulations for upper mantle peridotites with application to the thermobarometry of fertile lherzolite and garnet websterite, *Neues Jahrb. Mineral. Abh.*, *172*(2-3), 381–408.
Timm, C., K. Hoernle, P. van den Bogaard, I. Bindemann, and S. D. Weaver (2009), Geochemical evolution of intraplate volcanism at Banks Peninsula, New Zealand: Interaction between asthenospheric and lithospheric melts, *J. Petrol.*, *50*, 989–1023.
Timm, C., K. Hoernle, R. Werner, F. Hauff, P. van den Bogaard, J. White, N. Mortimer, and D. Garbe-Schönberg (2010), Temporal and geochemical evolution of the Cenozoic intraplate volcanism of Zealandia, *Earth Sci. Rev. 98*, 38–64.

Tulloch, A. J., and D. L. Kimbrough (1989), The Paparoa Metamorphic Core Complex, New Zealand: Cretaceous extension associated with fragmentation of the Pacific margin of Gondwana, *Tectonics*, *8*(6), 1217–1234.

Tulloch, A. J., and S. Nathan (1990), Spinel harzburgite xenoliths in alkali basalt and camptonite from North Westland and southeast Nelson, *N. Z. J. Geol. Geophys.*, *33*(4), 529–534, New Zealand.

Tulloch, A. J., J. Ramezani, D. L. Kimbrough, K. Faure, and A. H. Allibone (2009a), U-Pb geochronology of mid-Paleozoic plutonism in western New Zealand: Implications for S-type granite generation and growth of the east Gondwana margin, *Geol. Soc. Am. Bull.*, *121*(9-10), 1236–1261.

Tulloch, A. J., J. Ramezani, N. Mortimer, J. Mortensen, P. van den Bogaard, and R. Maas (2009b), Cretaceous felsic volcanism in New Zealand and Lord Howe Rise (Zealandia) as a precursor to final Gondwana break-up, *Geol. Soc. Spec. Publ.*, *321*(1), 89–118.

Turnbull, I. M. (2000), *Geology of the Wakatipu Area, Institute of Geological and Nuclear Sciences 1:250000 Geological Map 18*.

van der Meer, Q. H. A., J. M. Scott, T. E. Waight, M. Sudo, A. Schersten, A. F. Cooper, and T. L. Spell (2013), Magmatism during Gondwana breakup; new geochronological data from Westland, New Zealand, *N. Z. J. Geol. Geophys.*, *56*, 229–242.

Vervoort, J. D., P. J. Patchett, J. Blichert-Toft, and F. Albarède (1999), Relationships between Lu-Hf and Sm-Nd isotopic systems in the global sedimentary system, *Earth Planet. Sci. Lett.*, *168*, 79–99.

Waight, T. E., S. D. Weaver, R. Maas, and G. N. Eby (1998a), Bimodal Late Cretaceous alkaline magmatism and the opening of the Tasman Sea: West Coast, South Island, New Zealand, *Aust. J. Earth Sci.*, *45*, 823–835.

Waight, T. E., S. D. Weaver, and R. J. Muir (1998b), Mid-Cretaceous granitic magmatism during the transition from subduction to extension in southern New Zealand: A chemical and tectonic synthesis, *Lithos 45*, 469–482.

Wallace, R. C. (1975), Mineralogy and petrology of xenoliths in a diatreme from South Westland, New Zealand, *Contrib. Mineral. Petrol.*, *49*(3), 191–199.

Weaver, S. D., and I. E. M. Smith (1989), New Zealand intraplate volcanism, in *Intraplate Volcanism in Eastern Australia and New Zealand*, edited by R. W. Johnston, pp. 157–188, Cambridge University Press.

Witt-Eickschen, G., H. A. Seck, K. Mezger, S. M. Eggins, and R. Altherr (2003), Lithospheric mantle evolution beneath the Eifel (Germany): Constraints from Sr–Nd–Pb isotopes and trace element abundances in spinel peridotite and pyroxenite xenoliths, *J. Petrol.*, *44*(6), 1077–1095.

Wittig, N., D. G. Pearson, S. Duggen, J. A. Baker, and K. Hoernle (2010), Tracing the metasomatic and magmatic evolution of continental mantle roots with Sr, Nd, Hf and Pb isotopes: A case study of Middle Atlas (Morocco) peridotite xenoliths, *Geochim. Cosmochim. Acta*, *74*(4), 1417–1435.

Wright, J. B. (1967), Contributions to the volcanic succession and petrology of the Auckland Islands. II. Upper parts of the Ross Volcano, *Trans. R. Soc. N. Z. Geol.*, *5*, 71–87.

Yaxley, G. M., D. H. Green, and V. Kamenetsky (1998), Carbonatite metasomatism in the southeastern Australian lithosphere, *J. Petrol.*, *39*(11-12), 1917–1930.

Zhang, M., P. J. Stephenson, S. Y. O'Reilly, M. T. McCulloch, and M. Norman (2001), Petrogenesis and geodynamic implications of late Cenozoic basalts in North Queensland, Australia: Trace-element and Sr–Nd–Pb isotope evidence, *J. Petrol.*, *42*(4), 685–719.

Zindler, A., and S. Hart (1986), Chemical geodynamics, *Annu. Rev. Earth Planet. Sci.*, *14*, 493–571.